

TECHNICAL REPORT 1962
October 2007

Fano Bounds for Compact Antennas

Phase I

J. C. Allen
J. Meloling

Approved for public release;
distribution is unlimited.



SSC San Diego
San Diego, CA 92152-5001

Report Documentation Page				Form Approved OMB No. 0704-0188	
Public reporting burden for the collection of information is estimated to average 1 hour per response, including the time for reviewing instructions, searching existing data sources, gathering and maintaining the data needed, and completing and reviewing the collection of information. Send comments regarding this burden estimate or any other aspect of this collection of information, including suggestions for reducing this burden, to Washington Headquarters Services, Directorate for Information Operations and Reports, 1215 Jefferson Davis Highway, Suite 1204, Arlington VA 22202-4302. Respondents should be aware that notwithstanding any other provision of law, no person shall be subject to a penalty for failing to comply with a collection of information if it does not display a currently valid OMB control number.					
1. REPORT DATE OCT 2007		2. REPORT TYPE		3. DATES COVERED 00-00-2007 to 00-00-2007	
4. TITLE AND SUBTITLE Fano Bounds for Compact Antennas Phase I				5a. CONTRACT NUMBER	
				5b. GRANT NUMBER	
				5c. PROGRAM ELEMENT NUMBER	
6. AUTHOR(S)				5d. PROJECT NUMBER	
				5e. TASK NUMBER	
				5f. WORK UNIT NUMBER	
7. PERFORMING ORGANIZATION NAME(S) AND ADDRESS(ES) SPAWAR Systems Center San Diego, 53560 Hull Street, San Diego, CA, 92152-5001				8. PERFORMING ORGANIZATION REPORT NUMBER	
9. SPONSORING/MONITORING AGENCY NAME(S) AND ADDRESS(ES)				10. SPONSOR/MONITOR'S ACRONYM(S)	
				11. SPONSOR/MONITOR'S REPORT NUMBER(S)	
12. DISTRIBUTION/AVAILABILITY STATEMENT Approved for public release; distribution unlimited					
13. SUPPLEMENTARY NOTES					
14. ABSTRACT					
15. SUBJECT TERMS					
16. SECURITY CLASSIFICATION OF:			17. LIMITATION OF ABSTRACT Same as Report (SAR)	18. NUMBER OF PAGES 76	19a. NAME OF RESPONSIBLE PERSON
a. REPORT unclassified	b. ABSTRACT unclassified	c. THIS PAGE unclassified			

EXECUTIVE SUMMARY

Impedance matching is a canonical problem in electrical engineering—design a matching network that transfers maximum power from a generator to a load. Although the loads in this report are restricted to compact antennas, the mathematical exposition applies to any lumped load.

Finding a “good” matching network is a difficult numerical optimization problem. Therefore, techniques that compute bounds on the matching provide valuable information. For example, the *Fano bounds* discussed in this report bound the matching performance as a function of the frequency band. Therefore, the circuit design can see the matching performance against the bandwidth to make design decisions—without having to solve countless matching problems. Moreover, the Fano bounds provide an excellent benchmark to assess the performance of actual matching circuits—getting “close enough” to the best bounds is “good enough.”

The Fano bounds are computed by maximizing the matching performance under inequality constraints. The inequality constraints are determined by analytic expansions of the load. Because symbolic manipulators compute these expansions and the numerical packages can solve the inequality constraints, the Fano bounds may be amenable to a “hands-free” computation. However, the sticking point for the Fano bounds is the requirement that the load be given in the Darlington representation. Therefore, this Phase I effort shows that the Fano bounds can automate and defers the Darlington computation to Phase II.

Contents

Executive Summary	iii
1 Antenna Systems	1
2 Fano's Approach to Wideband Matching	7
3 Bode theorems	13
4 Gain-Bandwidth Bounds	22
5 RLC Fano Bounds (Unit Resistor)	26
6 RLC Fano Bounds (Arbitrary Resistor)	31
7 Microstrip Patch Antenna	34
8 Ideal Dipole	43
9 Automating the Fano Bounds	51
A Fano-Bode Integrals	52
B Scattering Measurements to a Darlington Representation	57
References	68

List of Figures

1	The 2-port scattering formalism.	5
2	Reflectances and powers.	7
3	Matching 2-port and Darlington's representation of the load. .	11
4	Bode integrand for Example 1.	14
5	Bode integrand of the reflectance of Example 2.	17
6	RL load.	23
7	Gain-bandwidth for the RL load.	24
8	Low-pass RLC load.	25
9	Low-pass RLC load with 1-ohm normalization.	26
10	Upper bounds on gain as a function of bandwidth $\omega_c = 2\pi\Delta f$. .	30
11	Lower bounds on VSWR as a function of bandwidth $\omega_c = 2\pi\Delta f$. .	30
12	Non-normalized low-pass RLC load.	31
13	Low-pass RLC load normalized to 50 ohms.	31
14	Upper bounds on gain as a function of bandwidth $\omega_c = 2\pi\Delta f$. .	33
15	Lower bounds on VSWR as a function of bandwidth $\omega_c = 2\pi\Delta f$. .	33
16	Microstrip patch antenna—equivalent circuit.	34
17	Microstrip patch antenna—impedance.	35
18	Microstrip patch antenna—reflectance.	36
19	Microstrip patch antenna—Fano 1-bound.	40
20	Microstrip patch antenna— K plot; 600–1100 MHz.	41
21	Impedance models of the TM_1 and TE_1 modes of the ideal dipole; $C = a\epsilon_0 = a \times 8.85$ (pF), $L = a\mu_0 = a \times 1.26$ (μ H), $R = \sqrt{\mu_0/\epsilon_0} = 377.3233$ (ohms).	43
22	Ideal dipole—impedance of the TM_1 mode.	44
23	Ideal dipole—VSWR of the TM_1 mode.	45
24	Ideal dipole—reflectance.	46
25	Ideal dipole— $K(u_1, v_1)$ plot.	49
26	Ideal dipole—Fano bounds.	50
27	Contour C_r , line segment L_r , half circle H_r	53
28	Surface Current Probe approximation with degree 4.	57
29	State-space representation of a passive, lumped N -port con- taining d reactive elements and r resistors.	58
30	AOC21B and approximation with degree 8.	62
31	AOC21B and approximation with degree 16.	63
32	CVN77Z approximation with degree 4.	64
33	CVN77Z approximation with degree 10.	65

34	CVN77Z approximation with degree 16.	66
35	Surface Current Probe (no transformer) approximation with degree 4.	67

List of Tables

1	Table of notation.	6
2	MATLAB [®] code evaluating Example 1.	15
3	MATLAB [®] code evaluating Example 2.	17
4	MATLAB [®] code evaluating Example 4.	21
5	Fano functions near the \mathbf{v} axis.	42
6	Extrema of the Lagrangian without positivity constraints. . .	48
7	Positive extrema of the Lagrangian.	49

1 Antenna Systems

The key idea for antenna design is that both the antenna and its matching circuit are the objects under design—not the antenna with the matching circuit as an afterthought. This point is developed in Zhu and Qi [30]:

The “raw” impedance characteristic of an antenna ... does not provide a ready index to what might be described as the “broad-band potential” of the antenna.

The notion of an *antenna system* is found in Gustafsson and Nordebo [13]:

The bandwidth of an antenna system can, in general, only be determined if this impedance is known for all frequencies in the considered frequency range. However, even if the impedance is known, the bandwidth depends on the specified threshold level of the reflection coefficient and the use of matching networks.

This notion of an “antenna system” is unavoidable when designing integrated systems such as transmit/receive modules and multiple-input/multiple-output systems. For example, a wideband microstrip circulator connected to an antenna requires a new design methodology [29]:

that allows for ... a single matching network that interfaces between the circulator and the antenna ...

In more detail, matching networks trade isolation between the transmitter and receiver against power transfer between the transmitter and the antenna, and the antenna and receiver. More generally, the limited bandwidth of the circulator forces the designer to trade power transfer and isolation to get more bandwidth. Consequently, antenna “tweaking” is a poor design approach for these integrated systems.

Basic to the performance of any antenna system are the matching networks. Classically, these matching networks are designed to optimize power transfer. This classic design objective is expanding to encompass multiple design objectives—increasing bandwidth [16], [2], increasing channel capacity

[18], reducing bit error rate [27], [6]. In any optimization problem, knowing global “best bounds” provides a benchmark to assess designs, terminate the numerical optimizers, and end the interminable “tweaking” by the engineers. The best matching performance is currently computed by the following techniques:

- Analytic matching theory of Fano [9] or Youla [28],
- H^∞ methods of Helton [14],
- Real-frequency technique of Carlin and Civalleri [5],
- Analytic bounds of Wohlers [26],
- Impedance disks of Sokolov, Babak and Babak [24].

A complete report would compare these methods on real antennas. Phase I starts this process with the Fano Method. The immediate objective is to implement Fano’s integral expansions in a symbolic calculator. The long-range objective is to automate the Fano Method to compute matching bounds starting from numerical antenna measurements.

Section 2 makes explicit the assumptions behind the key inequality obtained by Fano in his 1950 thesis [9]:

$$1 - G_T \geq |s_X|^2.$$

This inequality shows the transducer power gain G_T of *any* matching network is bounded by the Fano reflectance s_X extracted from a *Darlington’s representation* of the load. Consequently, the Fano reflectance from the *fixed* load limits the best possible gain achievable by any lossless matching network selected by the circuit designer.

The gain-bandwidth bounds are computed by evaluating integrals of the form:

$$\int_0^\infty \log(|s_X(j\omega)|^{-1}) d\omega = \frac{\pi}{2} A_1^\infty - \pi \sum p_m.$$

Section 3 reviews a convenient mathematical technique to evaluate these integrals. Appendix A examines this expansion to clarify the treatment of the DC term. Comparison is made with the symbolic calculators used throughout this report for automating the Fano computations.

Section 4 combines the integral techniques with the Fano inequality to develop Fano's gain-bandwidth bound:

$$-\frac{\omega_{\max} - \omega_{\min}}{2} \log(1 - G_{\max}) \leq \int_0^\infty \log(|s_X(j\omega)|^{-1}) d\omega,$$

where G_{\max} denotes the maximum gain attainable over the frequency band $\Omega = [\omega_{\min}, \omega_{\max}]$. Section 5 works out the Fano bounds restricted to a normalized resistor. Section 6 drops the normalization constraint so that the Fano bounds for antenna matching can be computed.

A Fano analysis for a microstrip patch antenna and ideal dipole is undertaken in Sections 7 and 8, respectively. The careful development provides a more flexible approach to the Fano bounds. Indeed, the literature typically obtains the Fano bound from a system of equality constraints. For example, one system has the form

$$\begin{aligned} \frac{\pi K}{2}(\omega_{\max} - \omega_{\min}) &= \int_0^\infty \log(|s_X(j\omega)|^{-1}) d\omega, \\ \frac{\pi K}{6}(\omega_{\max}^3 - \omega_{\min}^3) &= \int_0^\infty \omega^2 \log(|s_X(j\omega)|^{-1}) d\omega, \end{aligned}$$

where K is standard notation for the normalized bound on the Fano load over the frequency band:

$$\min\{\log(|s_X(j\omega)|^{-1}) : \omega \in \Omega\} =: \pi K/2.$$

The Fano bound is computed by solving for these equality constraints for K and then backing out the transducer power gain. As long as the two integrals are transverse with respect to K , a unique solution exists. This approach breaks down as additional constraints are derived. Unfortunately, "solutions" found in the literature are computed by tossing all but two of the equality constraints to obtain a sub-optimal bound. However, the Fano bound is really constrained by a *system of inequalities*. In terms of the preceding example, the Fano bound is computed by maximizing K subject to the inequalities:

$$\begin{aligned} \frac{\pi K}{2}(\omega_{\max} - \omega_{\min}) &\leq \int_0^\infty \log(|s_X(j\omega)|^{-1}) d\omega, \\ \frac{\pi K}{6}(\omega_{\max}^3 - \omega_{\min}^3) &\leq \int_0^\infty \omega^2 \log(|s_X(j\omega)|^{-1}) d\omega. \end{aligned}$$

An optimization problem with inequality constraints is a special case of the Kuhn-Tucker theory [17, Section 9.4]. Because the Kuhn-Tucker theory was not formalized until 11 years after Fano’s 1950 thesis, it appears that the special-case solutions obtained from the system of equalities have been conflated with the solutions to the general system of inequalities. In this report, the antenna examples compute the Fano bounds by carefully working through the inequality constraints.

Two major problems impede a “hands-free” implementation of the Fano bounds for real-world antenna-matching problems:

1. Integral expansions must be automated.
2. Numerical antenna measurements must be mapped into its Darlington’s representation.

Section 9 discusses both problems in detail and sets out the approach for Phase II. The symbolic calculations used in this report, coupled with restricting the load to antennas, demonstrate that the integral expansions can be automated—albeit a non-trivial piece of programming.

The problem mapping of a finite number of antenna measurements to a Darlington representation is more difficult. For example, the Fano bounds for some loads are based on the expansion of the reflectance $s_X(p)$ at $p = \infty$. Consequently, both the presence of the transmission zero at $p = \infty$ and its order must be extracted from the numerical measurements—and *a priori* knowledge of the antenna’s high-frequency behavior. Appendix B demonstrates that a Darlington’s representation can be obtained from sampled antenna measurements. The quality of this representation can be enhanced by incorporating *a priori* knowledge of the antenna—especially its behavior at high and low frequencies. Finally, progress made in mapping the antenna measurements carry over to other impedance-matching methods, especially the H^∞ methods that also rely on knowledge of the load over all frequencies.

The notation is the standard *scattering formalism* and illustrated in Figure 1. The voltage and current vectors

$$\mathbf{v} = \begin{bmatrix} v_1 \\ v_2 \end{bmatrix} \quad \mathbf{i} = \begin{bmatrix} i_1 \\ i_2 \end{bmatrix}$$

of the 2-port determine the *incident wave* [3, Eq. 4.25a], [4, page 234]

$$\mathbf{a} = \begin{bmatrix} a_1 \\ a_2 \end{bmatrix} = \frac{1}{2} \{ R_0^{-1/2} \mathbf{v} + R_0^{1/2} \mathbf{i} \} \quad (1)$$

and the *reflected wave* [3, Eq. 4.25b], [4, page 234]

$$\mathbf{b} = \begin{bmatrix} b_1 \\ b_2 \end{bmatrix} = \frac{1}{2} \{ R_0^{-1/2} \mathbf{v} - R_0^{1/2} \mathbf{i} \}, \quad (2)$$

with respect to the normalizing¹ matrix

$$R_0 = \begin{bmatrix} r_0 & 0 \\ 0 & r_0 \end{bmatrix}.$$

Consequently, the scattering matrix S maps the incident wave \mathbf{a} to the reflected wave \mathbf{b}

$$\mathbf{b} = \begin{bmatrix} b_1 \\ b_2 \end{bmatrix} = \begin{bmatrix} s_{11} & s_{12} \\ s_{21} & s_{22} \end{bmatrix} \begin{bmatrix} a_1 \\ a_2 \end{bmatrix} = S\mathbf{a}.$$

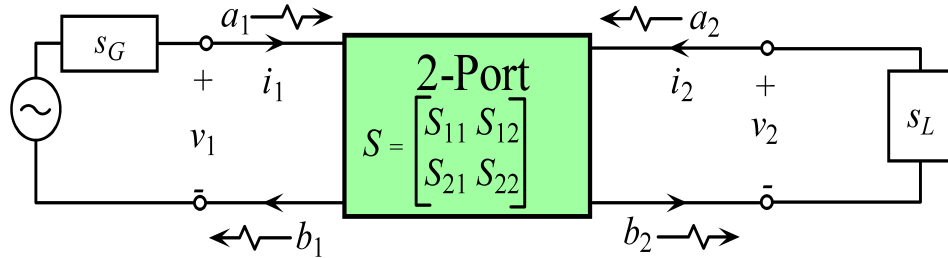


Figure 1: The 2-port scattering formalism.

The scattering matrix determines the impedance matrix Z as

$$\tilde{Z} := R_0^{-1/2} Z R_0^{-1/2} = (I + S)(I - S)^{-1},$$

¹Two accessible books on the scattering parameters are Baher [3] and Balabanian & Bickart [4]. Baher omits the factor of 1/2 but carries this rescaling onto the power definitions. Most other books use the *power-wave normalization* [8]: $\mathbf{a} = R_0^{-1/2} \{ \mathbf{v} + Z_0 \mathbf{i} \} / 2$, where the normalizing matrix $Z_0 = R_0 + jX_0$ is diagonal with diagonal resistance $R_0 > 0$ and reactance X_0 .

provided $I - S$ is invertible. Here \tilde{Z} denotes the normalized impedance matrix. If the N -port admits an impedance matrix Z ,

$$S = (\tilde{Z} - I)(\tilde{Z} + I)^{-1}.$$

Table 1 summarizes the notation.

Table 1: Table of notation.

Symbol	Description
j	$\sqrt{-1}$
p	Complex frequency: $p = \sigma + j\omega$
ω	Radial frequency
f	Frequency (Hertz): $\omega = 2\pi f$
σ	Neper frequency
\Re	Real part: $\Re[p] = \sigma$
\Im	Imaginary part: $\Im[p] = \omega$
\mathbb{R}	Real numbers
\mathbb{C}	Complex numbers
\mathbb{C}_+	Open right half plane
$j\mathbb{R}$	Imaginary axis
r_0	Normalizing resistance
s_L	Reflectance of the load
s_G	Reflectance of the generator
s_X	Fano reflectance
S	Scattering matrix
z_L	Impedance of the load
z_X	Fano impedance
Z	Impedance matrix

2 Fano's Approach to Wideband Matching

Most impedance matching techniques look *into the load*. In contrast, Fano looks *out from the load* to compute fundamental limitations on wideband matching. Specifically, Fano uses Darlington's theorem to compute wideband matching bounds over the class of all lossless, lumped 2-ports. This section reviews the lossless 2-port theory to implement Fano's view. Figure 2 shows the incident waves, reflected waves, and power flows of a 2-port with scattering matrix

$$S(p) = \begin{bmatrix} s_{11}(p) & s_{12}(p) \\ s_{21}(p) & s_{22}(p) \end{bmatrix} \quad (p = \sigma + j\omega)$$

that connects a generator to a load.

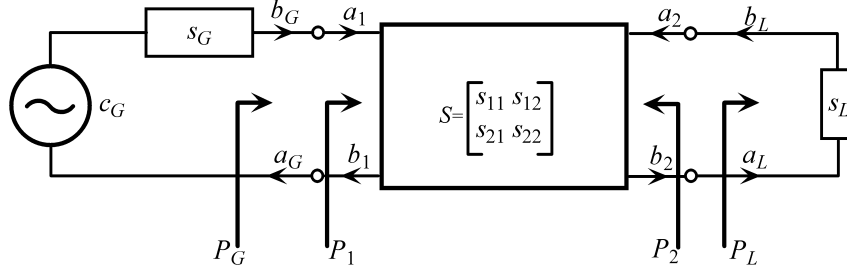


Figure 2: Reflectances and powers.

The 2-port is called *lossless*, provided S is unitary over all frequencies:

$$S(j\omega)^H S(j\omega) = \begin{bmatrix} 1 & 0 \\ 0 & 1 \end{bmatrix}.$$

The reflectance looking into Port 1 is

$$s_1 = \frac{b_1}{a_1} = s_{11} + s_{12}s_L(1 - s_{22}s_L)^{-1}s_{21} =: \mathcal{F}_1(S, s_L). \quad (3)$$

Similarly, the reflectance looking into Port 2 is

$$s_2 = \frac{b_2}{a_2} = s_{22} + s_{21}s_G(1 - s_{11}s_G)^{-1}s_{12} =: \mathcal{F}_2(S, s_G). \quad (4)$$

The power flows are determined from the incident and reflected waves:

- The average power delivered to Port 1:

$$P_1 := \frac{1}{2}(|a_1|^2 - |b_1|^2) = \frac{|a_1|^2}{2}(1 - |s_1|^2).$$

- The average power delivered to Port 2:

$$P_2 := \frac{1}{2}(|a_2|^2 - |b_2|^2) = -P_L.$$

- The average power delivered to the load [11, Eq. 2.6.6]:

$$P_L := \frac{1}{2}(|a_L|^2 - |b_L|^2) = \frac{|b_2|^2}{2}(1 - |s_L|^2).$$

- The average power delivered by the generator:

$$P_G = \frac{|c_G|^2}{2} \frac{1 - |s_1|^2}{|1 - s_G s_1|^2}.$$

The *maximum power available from a generator* is defined as the average power delivered by the generator to a conjugately matched load [11, Eq. 2.6.7]:

$$P_{G,\max} := P_G|_{s_1=\overline{s_G}} = \frac{|c_G|^2}{2}(1 - |s_G|^2)^{-1}.$$

The *source mismatch factor* [11, Eq. 2.7.17] is

$$\frac{P_G}{P_{G,\max}} = \frac{(1 - |s_G|^2)(1 - |s_1|^2)}{|1 - s_G s_1|^2}.$$

The *maximum power available from the 2-port* is defined as the average power delivered from the network to a conjugately matched load [11, Eq. 2.6.19]:

$$P_{L,\max} := P_L|_{s_L=\overline{s_2}} := \frac{|b_2|_{s_L=\overline{s_2}}^2}{2}(1 - |s_2|^2).$$

The *load mismatch factor* [11, Eq. 2.7.25] is

$$\frac{P_L}{P_{L,\max}} = \frac{(1 - |s_L|^2)(1 - |s_2|^2)}{|1 - s_L s_2|^2}.$$

The basic gains are itemized [11, page 213]:

- Transducer power gain:

$$G_T := \frac{P_L}{P_{G,\max}} = \frac{\text{power delivered to the load}}{\text{maximum power available from the generator}}.$$

- Power gain:

$$G_P := \frac{P_L}{P_1} = \frac{\text{power delivered to the load}}{\text{power delivered to the network}}.$$

- Available power gain:

$$G_A := \frac{P_{L,\max}}{P_{G,\max}} = \frac{\text{maximum power available from the network}}{\text{maximum power available from the generator}}.$$

When a general 2-port is used in Figure 2—be it lossless, passive, or active—the transducer power gain G_T is provided by Pozar [20, Eq. 11.13]:

$$G_T(s_G, S, s_L) = |s_{21}|^2 \frac{1 - |s_G|^2}{|1 - s_G s_1|^2} \frac{1 - |s_L|^2}{|1 - s_{22} s_L|^2}. \quad (5)$$

The *smallest* transducer power gain over a frequency band $\Omega = [\omega_{\min}, \omega_{\max}]$ is denoted:

$$\|G_T(s_G, S, s_L)\|_{\Omega, -\infty} := \sup\{G_T(s_G(j\omega), S(j\omega), s_L(j\omega)) : \omega \in \Omega\}.$$

The goal of impedance matching is to maximize the smallest transducer power gain:

Impedance Matching: Maximize the transducer power gain over a given a class \mathcal{S} of lossless 2-ports:

$$\sup\{\|G_T(s_G, S, s_L)\|_{\Omega, -\infty} : S \in \mathcal{S}\}.$$

Impedance matching admits several equivalent formulations. Define the *power mismatch* between reflectances s_1 and s_2 as [1]:

$$\Delta P(s_1, s_2) := \left| \frac{\overline{s_1} - s_2}{1 - s_1 s_2} \right|.$$

When the 2-port is lossless,

$$G_T(s_G, S, s_L) = 1 - \Delta P(s_G, s_1)^2 = 1 - \left| \frac{\overline{s_G} - s_1}{1 - s_G s_1} \right|^2. \quad (6)$$

Consequently, the power mismatch reveals the *conjugate matching* embedded in the transducer power gain. Moreover, a lossless 2-port admits matching at either Port 1 or at Port 2.

Lemma 1 [1] *If the 2-port of Figure 2 is lossless and $|s_1 s_G|, |s_2 s_L| < 1$,*

$$G_T(s_G, S, s_L) = 1 - \Delta P(s_G, s_1)^2 = 1 - \Delta P(s_2, s_L)^2.$$

The *largest* power mismatch over a frequency band $\Omega = [\omega_{\min}, \omega_{\max}]$ is denoted:

$$\|\Delta P(s_G, s_1)\|_{\Omega, \infty} := \sup \{ \Delta P(s_G(j\omega), s_1(j\omega)) : \omega \in \Omega \}.$$

Because the smallest transducer power gain is the largest power mismatch,

$$\|G_T(s_G, S, s_L)\|_{\Omega, -\infty} = 1 - \|\Delta P(s_G, s_1)\|_{\Omega, \infty}^2.$$

Consequently, *maximizing the smallest transducer power gain is equivalent to minimizing the largest power mismatch*. Fano [9] uses Darlington's theorem and Lemma 1 to untangle the load from the matching network.

Theorem 1 (Darlington) [26], [3] *Any rational bounded-real function is realized as the reflectance of a rational, lossless, reciprocal 2-port terminated in a 1-ohm resistor.*

Darlington's theorem provides a representation of the load's reflectance $s_L(p)$ as

$$s_L(p) = \mathcal{F}_1(S_L, 0; p),$$

where $S_L(p)$ is a 2×2 lossless scattering matrix terminated in a 1-ohm resistor. Figure 3 shows the matching 2-port connected to the load $s_L(p)$ given by Darlington's representation. It will be convenient to call the reflectance $s_X(p)$ looking in from the 1-ohm resistor the *Fano reflectance*. The transducer power gain $G_{T,X}$ from the generator to the 1-ohm resistor is

$$G_{T,X} = \frac{P_X}{P_{G,\max}} = \frac{P_L}{P_{G,\max}} \frac{P_X}{P_L} = G_T G_X,$$

where G_X is the power gain from the input of the load to the 1-ohm resistor.

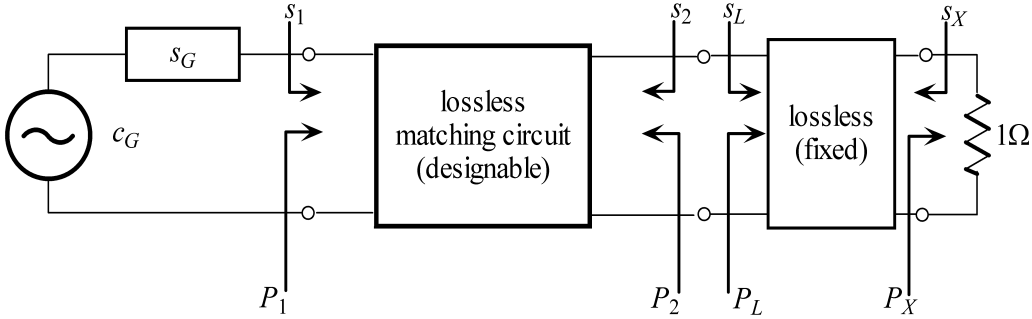


Figure 3: Matching 2-port and Darlington's representation of the load.

Because G_X never exceeds 1,

$$G_{T,X} \geq G_T. \quad (7)$$

Because both 2-ports are lossless, Lemma 1 links the Fano reflectance $s_X(p)$ to the transducer power gain:

$$G_{T,X} = 1 - \Delta P(s_X, 0)^2 = 1 - |s_X|^2 \geq G_T,$$

where the zero in the power mismatch implies the normalizing resistor is also 1-ohm. Consequently, the system loss is bounded by the Fano reflectance:

$$\boxed{1 - G_T \geq |s_X|^2.} \quad (8)$$

Because the matching network appears only in the gain, the Fano reflectance bounds the performance of any lossless matching network:

$$1 - \|s_X\|_\infty^2 \geq \sup\{\|G_T(s_G, S, s_L)\|_\infty : S \in \mathcal{S}\}.$$

This bound is a simple application of Equation 8. Fano uses the analyticity and structure of $s_X(p)$ to compute the more sophisticated gain-bandwidth bounds. The first-order bounds are obtained from the Bode theorems.

3 Bode theorems

If $h(p)$ is a rational function, the relative degree of $h(p)$ is denoted

$$\deg_r[h] = \# \text{ of zeros at infinity.}$$

Equivalently, if the relative degree of $h(p)$ is positive, $h(p)$ admits the expansion at infinity as

$$h(p) = \frac{h_{-1}}{p} + \frac{h_{-2}}{p^2} + \dots \quad (p \rightarrow \infty),$$

where the first non-zero term h_{-d} has index $d = \deg_r[h]$.

Theorem 2 (Bode Integral [12]) *Let $h(p)$ be a real rational function that admits an expansion at infinity as*

$$h(p) = \frac{h_{-1}}{p} + \frac{h_{-2}}{p^2} + \dots \quad (p \rightarrow \infty).$$

If $g(p) := (1 + h(p))^{-1}$ has neither zeros nor poles in the closed right half plane $\overline{\mathbb{C}}_+$,

$$\int_0^\infty \log(|g(j\omega)|) d\omega = -\frac{\pi}{2} h_{-1}.$$

Theorem 3 (Modified Bode Integral [12]) *Let $h(p)$ be a real rational function that admits an expansion at infinity as*

$$h(p) = \frac{h_{-1}}{p} + \frac{h_{-2}}{p^2} + \dots \quad (p \rightarrow \infty).$$

If $g(p) := (1 + h(p))^{-1}$ is analytic on $\overline{\mathbb{C}}_+$ and has zeros p_1, \dots, p_M in the open right half plane \mathbb{C}_+ ,

$$\int_0^\infty \log(|g(j\omega)|) d\omega = -\frac{\pi}{2} h_{-1} + \pi \sum_{m=1}^M p_m.$$

Example 1 (Single Pole) Let $a \in \mathbb{R}$ and define

$$h(p) = \frac{1}{p-a} = \frac{1}{p} + \frac{a}{p^2} + \frac{a^2}{p^3} + \frac{a^3}{p^4} + \dots \quad (p \rightarrow \infty).$$

The requirement that the integrand

$$g_a(p) = \frac{1}{1+h(p)} = \frac{p-a}{p-(a-1)}$$

be analytic on the closed right half plane forces $a < 1$. Theorem 3 computes

$$\int_0^\infty \log(|g_a(j\omega)|) d\omega = -\frac{\pi}{2} + \pi a.$$

Figure 4 plots the integrand when $a = 1/10$.

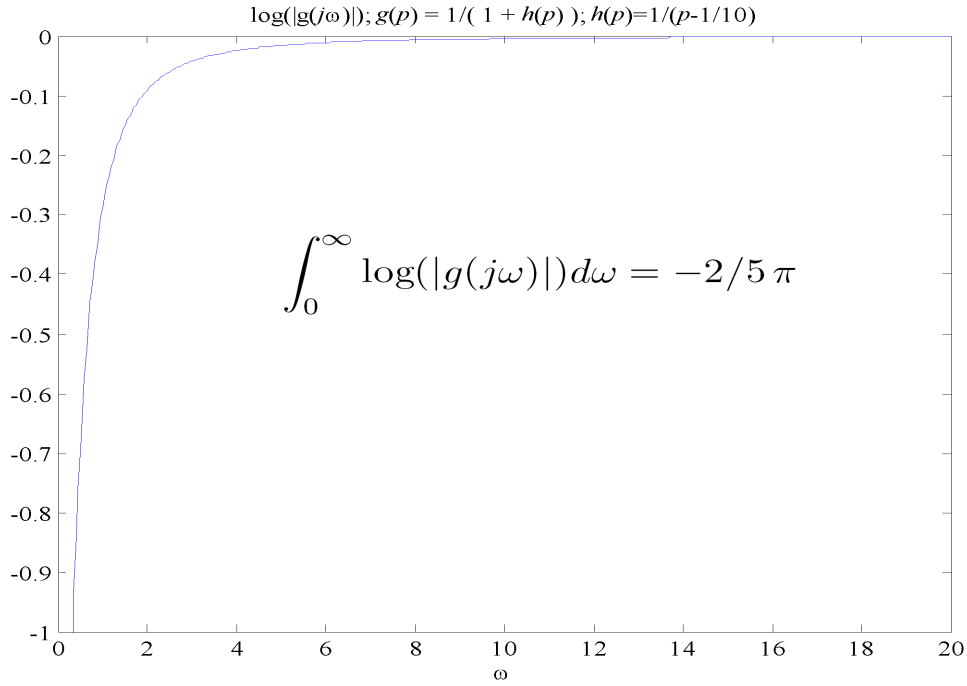


Figure 4: Bode integrand for Example 1.

The figure also shows the symbolic evaluation of the integral computed using the code listed Table 2.

Table 2: MATLAB[®] code evaluating Example 1.

```
syms p
syms w positive
h      = 1/(p - 1/10);
g      = 1/(1 + h);
gW     = subs(g,p,j*w);
gBIT   = int( log( abs(gW) ) , 0 , inf );
```

The first application of the Bode integral theorems mix the impedance and the scattering formalism for convenient evaluation of the Fano reflectance.

Corollary 1 *Let $z(p)$ is a real rational function with an expansion at infinity as*

$$z(p) = \frac{z_{-1}}{p} + \frac{z_{-2}}{p^2} + \dots \quad (p \rightarrow \infty).$$

If $g_{\pm}(p) := (1 \pm z(p))^{-1}$ are both analytic on $\overline{\mathbb{C}}_+$,

$$\int_0^{\infty} \log \left(\left| \frac{z(j\omega) - 1}{z(j\omega) + 1} \right| \right) d\omega = -\pi z_{-1}.$$

Proof: The Bode integral theorems can be applied to the sum of the logarithms. If $z(p) = u(p)/v(p)$ where $u(p)$ and $v(p)$ are real polynomials that are relatively prime,

$$g_{\pm}(p) = \frac{1}{1 \pm z(p)} = \frac{v(p)}{v(p) \pm u(p)}.$$

Because $u(p)$ and $v(p)$ are relatively prime, there can be no cancelation between $v(p)$ and $u(p) \pm v(p)$. Therefore,

$$\begin{aligned} \text{Zeros}[g_{\pm}] &= \text{Zeros}[v] \\ \text{Poles}[g_{\pm}] &= \text{Zeros}[u \pm v] \end{aligned}$$

Let p_1, \dots, p_M denote the zeros of $v(p)$ in the open right half plane. The assumption that $g_{\pm}(p)$ is analytic in the closed right half plane allows the Bode integral theorems to be applied:

$$\begin{aligned}
& \int_0^{\infty} \log \left(\left| \frac{z(j\omega) - 1}{z(j\omega) + 1} \right| \right) d\omega \\
&= \int_0^{\infty} \log(|z(j\omega) - 1|) d\omega - \int_0^{\infty} \log(|z(j\omega) + 1|) d\omega \\
&= - \int_0^{\infty} \log(|z(j\omega) - 1|^{-1}) d\omega + \int_0^{\infty} \log(|z(j\omega) + 1|^{-1}) d\omega \\
&= - \int_0^{\infty} \log(|g_-(j\omega)|) d\omega + \int_0^{\infty} \log(|g_+(j\omega)|) d\omega \\
&= - \left\{ -\frac{\pi}{2} \lim_{p \rightarrow \infty} p(-z(p)) + \pi \sum_{m=1}^M p_m \right\} \\
&\quad + \left\{ -\frac{\pi}{2} \lim_{p \rightarrow \infty} p(+z(p)) + \pi \sum_{m=1}^M p_m \right\} \\
&= -\pi z_{-1}
\end{aligned}$$

///

Example 2 *The expansion of $z(p)$ at infinity is*

$$z(p) = \frac{1}{p+3} = \frac{1}{p} - \frac{3}{p^2} + \frac{9}{p^3} - \dots \quad (p \rightarrow \infty)$$

and produces the reflectance

$$s(p) = \frac{z(p) - 1}{z(p) + 1} = \frac{g_+(p)}{g_-(p)},$$

where

$$g_+(p) = \frac{1}{z+1} = \frac{p+3}{p+4}$$

is analytic on $\overline{\mathbb{C}}_+$ with the single pole at $p = -4$ and

$$g_-(p) = \frac{1}{z-1} = -\frac{p+3}{p+2}$$

is analytic on $\overline{\mathbb{C}}_+$ with the single pole at $p = -2$. Consequently, Corollary 1 applies and computes the integrand as $-\pi$.

Figure 5 plots the integrand and displays the symbolic computation obtained from the code listed in Table 3.

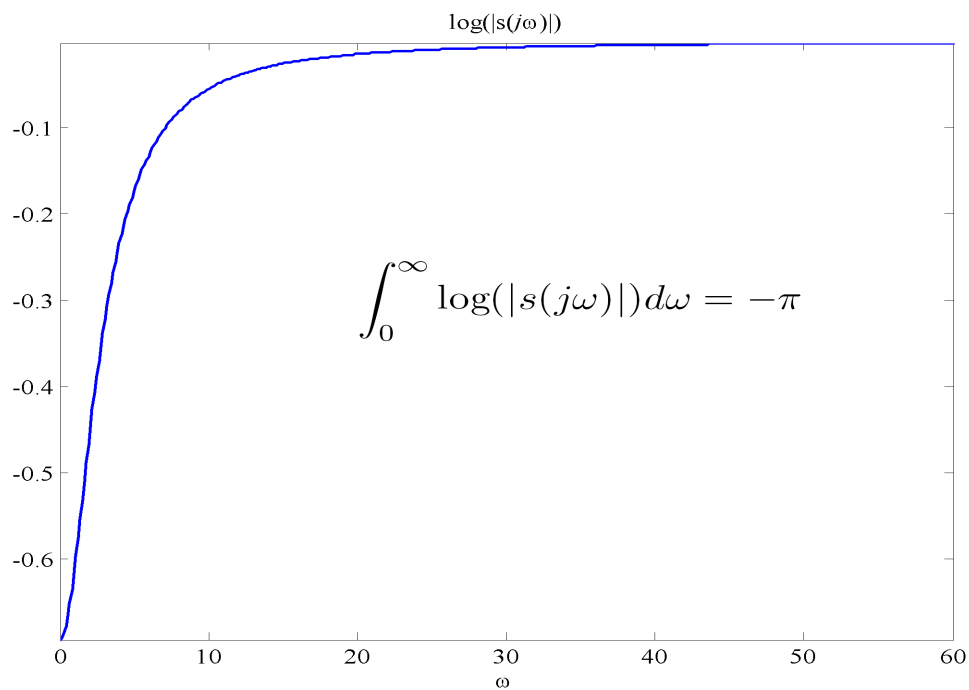


Figure 5: Bode integrand of the reflectance of Example 2.

Table 3: MATLAB[®] code evaluating Example 2.

```
syms p
syms w positive
z = 1/( p + 3);
sW = simplify( subs( (z-1)/(z+1) , p , j*w ));
gBIT = int( log( abs(sW) ) , 0 , inf )
```

A more flexible computation splits the integrand and accepts separate right and left half plane analyticity.

Corollary 2 *Let $z(p)$ be a real rational function with an expansion at infinity as*

$$z(p) = \frac{z_{-1}}{p} + \frac{z_{-2}}{p^2} + \dots \quad (p \rightarrow \infty).$$

If $g_{\pm}(p) := (1 \pm z(p))^{-1}$ is analytic on $\overline{\mathbb{C}}_{\pm}$,

$$\int_0^{\infty} \log \left(\left| \frac{z(j\omega) - 1}{z(j\omega) + 1} \right| \right) d\omega = -\pi z_{-1} + \pi \sum p_m,$$

where the p_m 's are the poles of $z(p)$.

Proof: The Bode integral theorems apply to the sum of the logarithms. Let $z = u/v$ be real polynomials that are relatively prime.

$$g_{\pm} = \frac{1}{1 \pm z} = \frac{v}{v \pm u}.$$

Because $u(p)$ and $v(p)$ are relatively prime, there can be no cancelation between $v(p)$ and $u(p) \pm v(p)$. Therefore,

$$\begin{aligned} \text{Zeros}[g_{\pm}] &= \text{Zeros}[v] \\ \text{Poles}[g_{\pm}] &= \text{Zeros}[u \pm v] \end{aligned}.$$

Let p_n^{\pm}, \dots denote the zeros of $v(p)$ in the open \mathbb{C}_{\pm} . The Bode integral theorems adapt to $g_{-}(p)$ using the observation that

$$g_{*}(p) := g_{-}(-p) = \frac{1}{1 - z(-p)}$$

is analytic on the open right half plane. The Bode integral theorems compute

$$\begin{aligned} \int_0^{\infty} \log |g_{-}(j\omega)| d\omega &= - \int_0^{\infty} \log |g_{-}(-j\omega)| d\omega \\ &= - \left\{ -\frac{\pi}{2} \lim_{p \rightarrow \infty} p(-z(-p)) + \pi \sum p_m^{-} \right\} \\ &= - \left\{ -\frac{\pi}{2} z_{-1} + \pi \sum p_m^{-} \right\} \\ &= +\frac{\pi}{2} z_{-1} - \pi \sum p_m^{-}. \end{aligned}$$

Applied to the reflectance, the Bode integral theorems compute

$$\begin{aligned}
& \int_0^\infty \log \left(\left| \frac{z(j\omega) - 1}{z(j\omega) + 1} \right| \right) d\omega \\
&= \int_0^\infty \log(|z(j\omega) - 1|) d\omega - \int_0^\infty \log(|z(j\omega) + 1|) d\omega \\
&= - \int_0^\infty \log(|z(j\omega) - 1|^{-1}) d\omega + \int_0^\infty \log(|z(j\omega) + 1|^{-1}) d\omega \\
&= - \int_0^\infty \log |g_-(j\omega)| d\omega + \int_0^\infty \log(|g_+(j\omega)|) d\omega \\
&= - \left\{ +\frac{\pi}{2} z_{-1} - \pi \sum p_m^- \right\} \\
&\quad + \left\{ -\frac{\pi}{2} z_{-1} + \pi \sum p_m^+ \right\} \\
&= -\pi z_{-1} + \pi \sum p_m^+ + \pi \sum p_m^-.
\end{aligned}$$

///

The Bode integral theorems apply to the scattering integrand when $z(p)$ is unbounded. The next result only needs one pole condition and admits several useful computations.

Corollary 3 *Suppose $z(p)$ is a lumped impedance—a positive real rational function—that admits an expansion at infinity as*

$$z(p) = z_1 p + z_2 p^2 + \dots \quad (p \rightarrow \infty).$$

Observe that the reflectance

$$s(p) := \frac{z(p) - 1}{z(p) + 1}$$

is analytic on $\overline{\mathbb{C}_+}$. Let p_1, \dots, p_M in \mathbb{C}_+ denote the zeros of $s(p)$ in \mathbb{C}_+ . Then

$$\int_0^\infty \log(|s(j\omega)|) d\omega = -\pi \lim_{p \rightarrow \infty} \frac{p}{z(p) - 1} + \pi \sum_{m=1}^M p_m.$$

Proof: Write

$$g(p) := \frac{z(p) - 1}{z(p) + 1} = \frac{1}{1 + h(p)} \implies h(p) = \frac{2}{z(p) - 1}.$$

Observe that if $h(p) = u(p)/v(p)$,

$$g(p) = \frac{u(p) - v(p)}{u(p) + v(p)}.$$

Because $u(p)$ and $v(p)$ are relatively prime, $(u(p) + v(p))$ and $(u(p) - v(p))$ are relatively prime. Therefore, there are no pole-zero cancelations between this numerator and denominator of $g(p)$ so that

$$\begin{cases} \text{Zeros}[g] = \text{Zeros}[u - v] \\ \text{Poles}[g] = \text{Zeros}[u + v] \end{cases}.$$

If $g(p)$ is analytic in the closed right half plane, Theorem 3 computes

$$\int_0^\infty \log(|g(j\omega)|) d\omega = -\frac{\pi}{2} h_{-1} + \pi \sum_{m=1}^M p_m.$$

Observe that

$$h_{-1} = \lim_{p \rightarrow \infty} p h(p) = 2 \lim_{p \rightarrow \infty} \frac{p}{z(p) - 1}$$

to get the final form. ///

Example 3 If $z(p) = p$,

$$s(p) = \frac{z(p) - 1}{z(p) + 1} = \frac{p - 1}{p + 1}$$

has a pole at -1 and a zero at $p_1 = 1$. Because $|s(j\omega)| = 1$, the integral of $\log(|s(j\omega)|^{-1})$ is zero. Corollary 3 computes

$$\int_0^\infty \log(|s(j\omega)|) d\omega = -\pi \lim_{p \rightarrow \infty} \frac{p}{z(p) - 1} + \pi p_1 = -\pi \lim_{p \rightarrow \infty} \frac{p}{p - 1} + \pi = 0.$$

Example 4 If $z(p) = p + p^2$,

$$s(p) = \frac{z(p) - 1}{z(p) + 1} = \frac{p^2 + p - 1}{p^2 + p + 1}$$

has poles in the left half plane and zeros in the right half plane:

Poles	Zeros
-0.5000 - 0.8660i	0.6180
-0.5000 + 0.8660i	-1.6180

A symbolic computation of the integral produces

$$\int_0^\infty \log(|s(j\omega)|)d\omega = \pi \frac{2}{\sqrt{5} + 1} = \pi \times 0.6180.$$

Corollary 3 computes

$$\begin{aligned} \int_0^\infty \log(|s(j\omega)|)d\omega &= -\pi \lim_{p \rightarrow \infty} \frac{p}{z(p) - 1} + \pi \sum_{m=1}^M p_m \\ &= 0 + \pi \times 0.6180. \end{aligned}$$

Table 4: MATLAB[®] code evaluating Example 4.

```
syms p
syms w positive
z = p + p^2;
s = simplify((z-1)/(z+1));
sW = simplify( subs( s , p , j*w ));
sBIT = int( log(abs(sW)) , 0, inf );
```

4 Gain-Bandwidth Bounds

The Bode integral theorems can be coupled with the Fano bound of Equation 8 to produce the classic gain-bandwidth bounds:

$$\begin{aligned}
1 - G_T &\geq |s_X|^2 \\
\iff \log(1 - G_T) &\geq 2 \log(|s_X|) \\
\iff -\log(1 - G_T) &\leq -2 \log(|s_X|) \\
\iff -\frac{1}{2} \log(1 - G_T) &\leq \log(|s_X|^{-1}).
\end{aligned}$$

Integrating this inequality produces the general gain-bandwidth integral constraints:

$$-\frac{1}{2} \int_0^\infty \log(1 - G_T(j\omega)) d\omega \leq \int_0^\infty \log(|s_X(j\omega)|^{-1}) d\omega.$$

As a special case, the classic gain profile

$$G_T(j\omega) = \begin{cases} G_{\max} & \omega_1 \leq \omega \leq \omega_2 \\ 0 & \text{otherwise} \end{cases},$$

simplifies the inequality to

$$-\frac{\omega_2 - \omega_1}{2} \log(1 - G_{\max}) \leq \int_0^\infty \log(|s_X(j\omega)|^{-1}) d\omega. \quad (9)$$

The Bode-Fano theorems bound the integral using the parameters of the Fano load $s_X(p)$. Consequently, the load itself bounds the maximum gain. For example, suppose the load is an inductor in series with a resistor as shown in Figure 6. The impedance looking in from the resistor

$$z_X(p) = pL_1 + z_2(p)$$

has reflectance normalized to the resistor

$$s_X(p) = \frac{z_X(p) - R}{z_X(p) + R}.$$

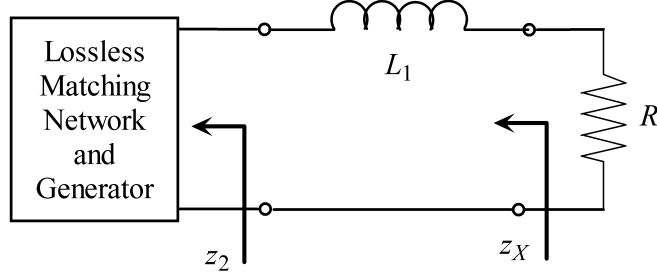


Figure 6: RL load.

If $z_2(p)$ is bounded as $p \rightarrow \infty$, Corollary 3 computes

$$\int_0^\infty \log(|s_X(j\omega)|^{-1}) d\omega = \pi \frac{R}{L_1} - \pi \sum_{m=1}^M p_m,$$

where the p_m 's are the zeros of $s_X(p)$ in the open right half plane. Combined with the classic gain of Equation 9, a Bode gain-bandwidth bound is obtained [20, page 262]:

$$-\frac{\Delta\omega}{2} \log(1 - G_{\max}) \leq \int_0^\infty \log(|s_X(j\omega)|^{-1}) d\omega \leq \frac{\pi R}{L_1}.$$

With $\Delta\omega = 2\pi\Delta f$, the gain-bandwidth bound is

$$-\Delta f \log(1 - G_{\max}) \leq \frac{R}{L_1}$$

and is plotted in Figure 7.

Now consider the load of Figure 8. The impedance looking in from the resistor [9, pages 71–73]

$$z_X(p) = pL_1 + (pC_2 + y_2(p))^{-1}$$

has reflectance $s_X(p) = (z_X(p) - R)(z_X(p) + R)^{-1}$ normalized to the resistor. If $y_2(p)$ is bounded as $p \rightarrow \infty$, Corollary 3 computes

$$\int_0^\infty \log(|s_X(j\omega)|^{-1}) d\omega = +\frac{\pi R}{L_1} - \pi \sum_{m=1}^M p_m.$$

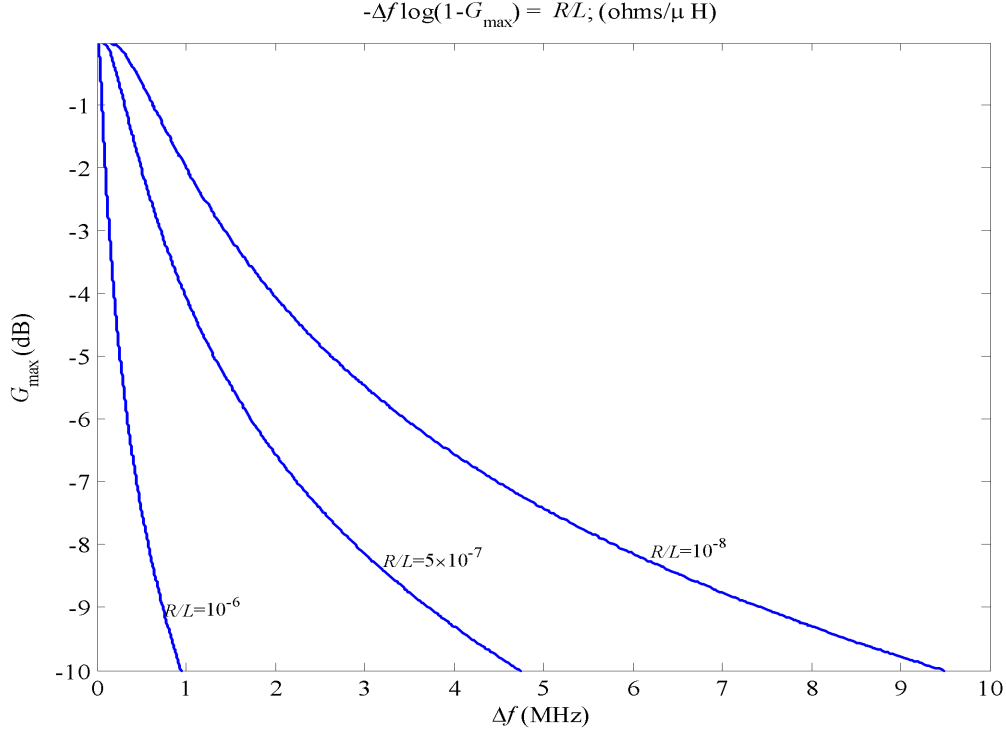


Figure 7: Gain-bandwidth for the RL load.

Although there is an additional capacitor, this bound is exactly the preceding RL bound. Fano's inspired solution was an adroit selection of *analytic windows* to exploit the hidden structure of the load. In this case, Fano observed that Darlington's representation of the load forces two transmission zeros at $p = \infty$. These transmission zeros force the expansion at infinity to have the form

$$\log(s_X(p)^{-1}) = \frac{A_1^\infty}{p} + \frac{A_3^\infty}{p^3} + \frac{A_4^\infty}{p^4} + \frac{A_5^\infty}{p^5} + \dots,$$

where the first two terms depend *only on the load*. The Bode integral really extracts A_1^∞ :

$$\int_0^\infty \log(|s_X(j\omega)|^{-1}) d\omega = +\frac{\pi}{2} A_1^\infty - \pi \sum_{m=1}^M p_m.$$

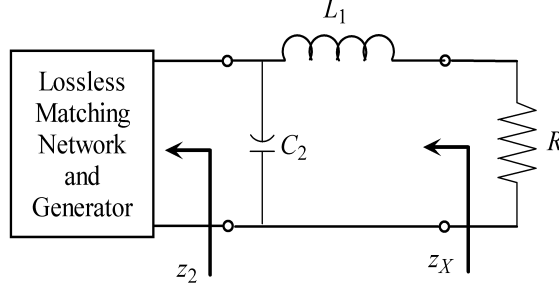


Figure 8: Low-pass RLC load.

Fano uses the quadratic window to extract A_3^∞ :

$$\int_0^\infty \omega^2 \log(|s_X(j\omega)|^{-1}) d\omega = -\frac{\pi}{2} A_3^\infty + \pi \sum_{m=1}^M p_m^3.$$

More generally, if the reflectance has an N transmission zeros at infinity, the expansion at infinity has the form [9, Eq. 9]

$$\log(s_X(p)^{-1}) = j\beta + \frac{A_1^\infty}{p} + \frac{A_3^\infty}{p^3} + \dots + \frac{A_{2N+1}^\infty}{p^{2N+1}} + \frac{A_{2N+2}^\infty}{p^{2N+2}} \dots,$$

where the leading odd coefficients depend *only on the lossless network of the load*. The corresponding windowed integrals are

$$\int_0^\infty \omega^{2n} \log(|s_X(j\omega)|^{-1}) d\omega = (-1)^n \frac{\pi}{2} \left\{ A_{2n+1}^\infty - \frac{2}{2n+1} \sum p_m^{2n+1} \right\},$$

for $n = 0, 1, \dots, N$. The next section works out the gain-bandwidth bounds for the RLC load in detail.

5 RLC Fano Bounds (Unit Resistor)

Fano's gain-bandwidth tradeoffs for the low-pass RLC load are derived in detail [9, pages 70–73]. Figure 9 shows the Darlington representation of the load and the Fano reflectance looking in from the 1-ohm resistor.

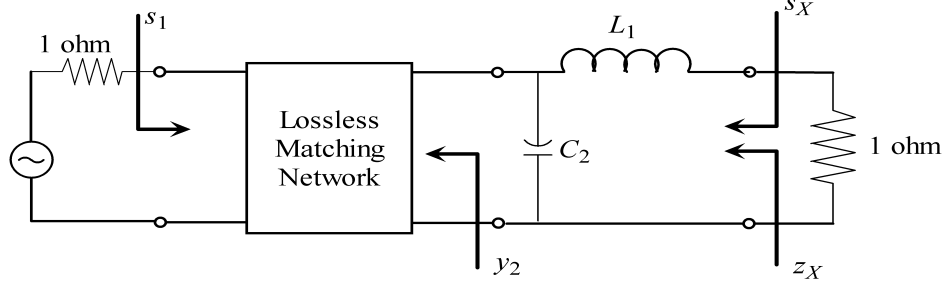


Figure 9: Low-pass RLC load with 1-ohm normalization.

The lossless part of the RLC load is a low-pass ladder of degree 2 with scattering matrix [9, Fig. 5]:

$$S_X(p) = \frac{\begin{bmatrix} p(pL_1C_2 + L_1 - C_2) & 2 \\ 2 & -p(pL_1C_2 + C_2 - L_1) \end{bmatrix}}{p^2L_1C_2 + p(L_1 + C_2) + 2}.$$

Consequently, there are two transmission zeros at $p = \infty$. The impedance looking in from the resistor [9, pages 71–73]

$$z_X(p) = pL_1 + (pC_2 + y_2(p))^{-1}$$

produces the Fano reflectance

$$s_X(p) = \frac{z_X(p) - 1}{z_X(p) + 1}$$

normalized to 1-ohm. The expansion of the integrand at infinity is

$$\begin{aligned} \log(s_X(p)^{-1}) &= \frac{A_1^\infty}{p} + \frac{A_3^\infty}{p^3} + \frac{A_4^\infty}{p^4} + \frac{A_5^\infty}{p^5} + \dots \\ &= \frac{2}{pL_1} + \frac{1}{p^3} \left\{ \frac{2}{3L_1^3} - \frac{2}{L_1^2C_2} \right\} + \frac{1}{p^4} \frac{2y_2(p)}{L_1^2C_2^2} + \mathcal{O}[p^{-5}], \end{aligned}$$

provided the admittance $y_2(p)$ is bounded as $p \rightarrow \infty$. The expansion shows that the load's transmission zeros push the matching network into the higher order terms. The two transmission zeros at infinity give the Fano equations [9, Table 1]:

$$\begin{aligned} \int_0^\infty \log(|s_X(j\omega)|^{-1})d\omega &= \frac{\pi}{2}A_1^\infty - \pi \sum p_m \\ \int_0^\infty \omega^2 \log(|s_X(j\omega)|^{-1})d\omega &= -\frac{\pi}{2}A_3^\infty + \frac{\pi}{3} \sum p_m^3, \end{aligned}$$

where the p_m 's are the zeros of $s_X(p)$ in the open right half plane. Denote the low-pass frequency band as $\Omega := [0, \omega_c]$. Bound the performance of the reflectance $s_X(p)$ on Ω as

$$\min\{\log(|s_X(j\omega)|^{-1}) : \omega \in \Omega\} =: \pi K/2.$$

Consequently, the reflectance $s_X(p)$ is bounded on the entire frequency axis as

$$\log(|s_X(j\omega)|^{-1}) \geq \begin{cases} \pi K/2 & |\omega| < \omega_c \\ 0 & |\omega| \geq \omega_c \end{cases}.$$

Inserting this lower bound into the two integrals produces the inequalities

$$\begin{aligned} \omega_c \pi K/2 &\leq \int_0^\infty \log(|s_X(j\omega)|^{-1})d\omega \\ \omega_c^3 \pi K/6 &\leq \int_0^\infty \omega^2 \log(|s_X(j\omega)|^{-1})d\omega. \end{aligned}$$

Combining these inequalities with the integral equations gives [9, Eq. 25, 26]

$$\begin{aligned} \omega_c K &\leq A_1^\infty - 2 \sum p_m \\ \omega_c^3 K &\leq -3A_3^\infty + 2 \sum p_m^3, \end{aligned}$$

The problem is to maximize K subject to these Fano equations. It was Fano's insight that equality is simultaneously achieved at maximum:

$$\begin{aligned} \omega_c K &= A_1^\infty - 2 \sum p_m \\ \omega_c^3 K &= -3A_3^\infty + 2 \sum p_m^3. \end{aligned}$$

Because the complex zeros p_m come in conjugate pairs, only the real part of the equations need to be retained:

$$\begin{aligned}\omega_c K &= A_1^\infty - 2 \sum u_m \\ \omega_c^3 K &= -3A_3^\infty + 2 \sum u_m^3 - 3u_m v_m^2,\end{aligned}$$

where complex frequency $p = u + jv$ determines that $\Re[p^3] = u^3 - 3uv^2$.

To formulate maximizing K as a standard optimization problem, maximize the first equation while enforcing equality between both equations. That is, maximize

$$K = h(\mathbf{u}, \mathbf{v}) = \frac{A_1^\infty}{\omega_c} - \frac{2}{\omega_c} \sum u_m$$

subject to the constraints $\mathbf{u} > 0$ and

$$g(\mathbf{u}, \mathbf{v}) = \left(\frac{A_1^\infty}{\omega_c} + 3 \frac{A_3^\infty}{\omega_c^3} \right) - \frac{2}{\omega_c} \sum u_m - \frac{2}{\omega_c^3} \sum u_m^3 - 3u_m v_m^2 = 0.$$

By the Lagrange multiplier theorem, if $h(\mathbf{u}, \mathbf{v})$ has a local extremum under that constraint $g(\mathbf{u}, \mathbf{v}) = 0$, the gradient of h is normal to the tangent space of the contours of the constraint function g [17, Section 9.8]:

$$\nabla h = \lambda \nabla g.$$

In this case,

$$\nabla h = -\frac{2}{\omega_c} \begin{bmatrix} \mathbf{u} \\ 0 \end{bmatrix} = \lambda \left\{ -\frac{2}{\omega_c} \begin{bmatrix} \mathbf{u} \\ 0 \end{bmatrix} - \frac{6}{\omega_c^3} \begin{bmatrix} \mathbf{u}^2 \\ 0 \end{bmatrix} + \frac{6}{\omega_c^3} \begin{bmatrix} \mathbf{v}^2 \\ 2\mathbf{u}\mathbf{v} \end{bmatrix} \right\} = \lambda \nabla g.$$

Because $\mathbf{u} > 0$, the \mathbf{v} component of the Lagrange equation forces $\mathbf{v} = 0$. Then the \mathbf{u} component of the Lagrange equation simplifies:

$$\mathbf{1} = \lambda \left\{ 1 + \frac{3}{\omega_c^2} \mathbf{u} \right\}.$$

That is, all the \mathbf{u} 's are equal. Equivalently, at an optimum value of K , there is a single positive zero u_0 that must satisfy [9, Eq. 27, 28]

$$g(u) = \left(\frac{A_1^\infty}{\omega_c} + 3 \frac{A_3^\infty}{\omega_c^3} \right) - \frac{2}{\omega_c} u - \frac{2}{\omega_c^3} u^3 = 0.$$

The single, real root u_0 of $g(u) = 0$ is

$$u_0 = 6^{-1}D^{1/3} - 2\omega_c^2 D^{-1/3},$$

where

$$D = 54A_1^\infty \omega_c^2 + 162A_3^\infty + 6\sqrt{48\omega_c^6 + 81A_1^{\infty 2}\omega_c^4 + 486A_1^\infty \omega_c^2 A_3^\infty + 729A_3^{\infty 2}}.$$

An optimal value of K is linked to the bandwidth ω_c as

$$K_{\text{opt}} = \frac{3A_1^\infty D^{1/3} - D^{2/3} + 12\omega_c^2}{\omega_c D^{1/3}}. \quad (10)$$

Taking the maximum of Equation 8 gives

$$1 - \|G_T\|_{\Omega, -\infty} \geq \|s_X\|_{\Omega, \infty}^2 = \exp(-\pi K_{\text{opt}}).$$

That is, the transducer power gain is bounded from above as

$$1 - \exp(-\pi K_{\text{opt}}) \geq \|G_T\|_{\Omega, -\infty}. \quad (11)$$

Figure 10 plots this upper bound on the transducer power gain as a function of bandwidth for nominal values of the inductor and capacitor. The plot shows that no matching circuit can deliver more than half power to the load ($G_T = -3$ dB) over the frequency band 0–0.32 MHz.

To plot the Voltage Standing Wave Ratio (VSWR) against bandwidth, observe that the input reflectance s_1 links to s_X as

$$|s_1(j\omega)|^2 = 1 - G_T(j\omega) \geq |s_X(j\omega)|^2$$

because the 1-ohm normalization sets $s_G = 0$. Taking the maximum yields

$$\|s_1\|_{\Omega, \infty} = \sup\{|s_1(j\omega)| : \omega \in \Omega\} \geq \|s_X\|_{\Omega, \infty} = \exp(-\pi K/2).$$

Because the VSWR is an increasing function,

$$\text{VSWR}(\|s_1\|_{\Omega, \infty}) \geq \text{VSWR}(\|s_X\|_{\Omega, \infty}) = \frac{1 + \exp(-\pi K/2)}{1 - \exp(-\pi K/2)}.$$

Consequently, the optimum K value provides the lower bound

$$\text{VSWR}(\|s_1\|_{\Omega, \infty}) \geq \frac{1 + \exp(-\pi K_{\text{opt}}/2)}{1 - \exp(-\pi K_{\text{opt}}/2)}. \quad (12)$$

Figure 11 plots this lower bound as a function of bandwidth. The plot shows that no matching circuit can be constructed that has a VSWR less than 3 over the frequency band 0–0.24 MHz.

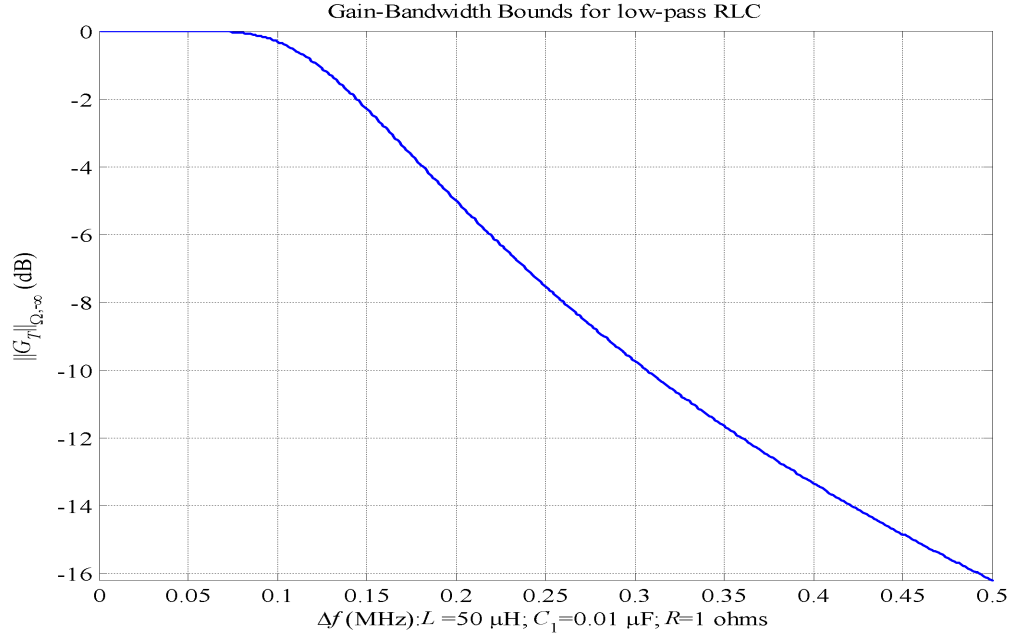


Figure 10: Upper bounds on gain as a function of bandwidth $\omega_c = 2\pi\Delta f$.

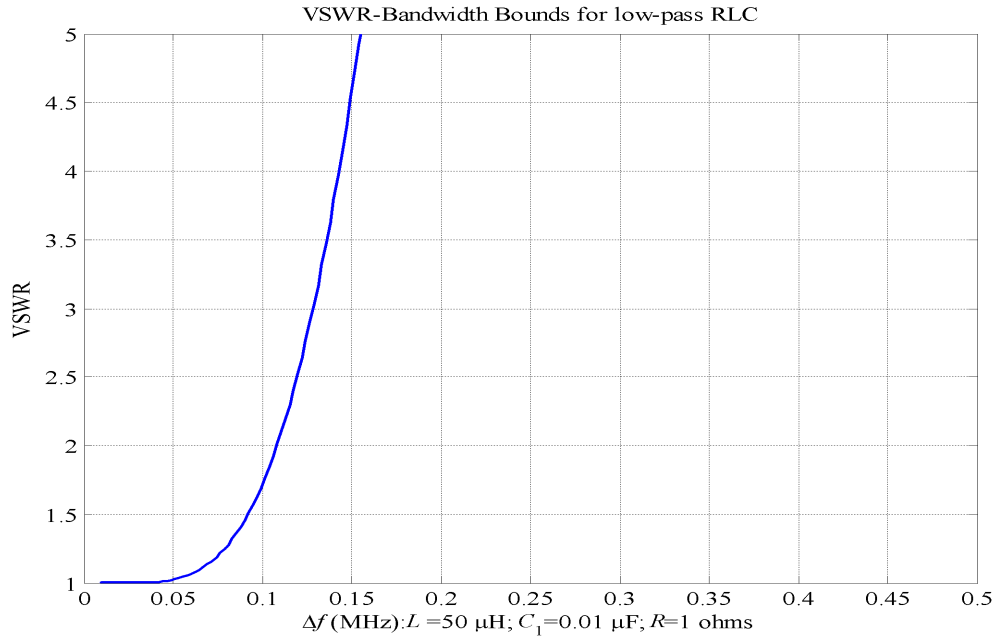


Figure 11: Lower bounds on VSWR as a function of bandwidth $\omega_c = 2\pi\Delta f$.

6 RLC Fano Bounds (Arbitrary Resistor)

Up to now, the load's resistor has been normalized out of the analysis. For practical systems, the normalization is typically set to 50 ohms while the resistive part of the load is determined by the physics of the system. Figure 12 shows a matching network with the generator's side normalized to $R_0 = 50$ ohms while the load has $R = 300$ ohms hanging on the end.

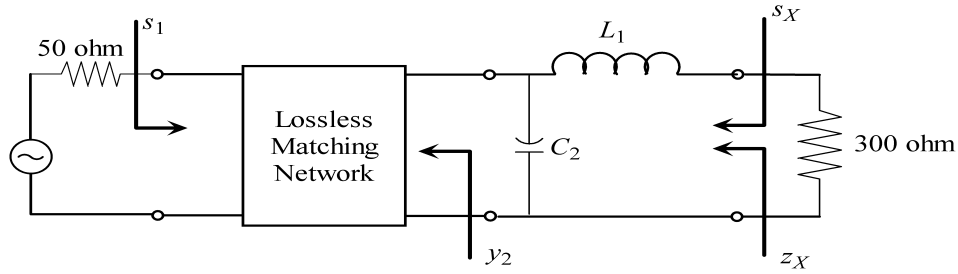


Figure 12: Non-normalized low-pass RLC load.

Fano [9] normalizes by a transformer as shown in Figure 13. Looking into the transformer from the matching network, the transformer has a chain matrix [3, page 20]

$$T = \begin{bmatrix} n^{-1} & 0 \\ 0 & n \end{bmatrix},$$

with winding number $n = \sqrt{R_0/R}$ to transform the R_0 into the load's resistance $R = R_0/n^2$.

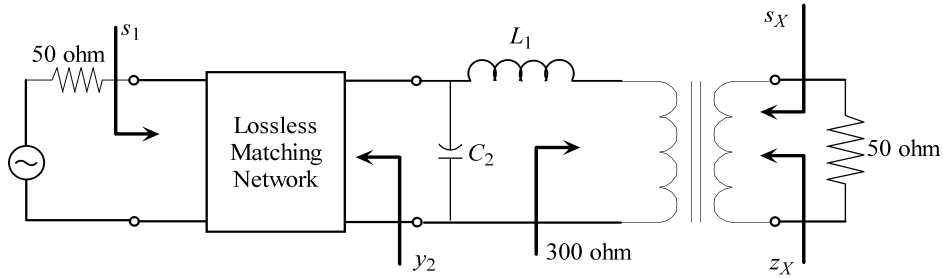


Figure 13: Low-pass RLC load normalized to 50 ohms.

Let $\tilde{z}_X(p)$ denote the impedance looking toward the generator from the input port of the transformer:

$$\tilde{z}_X(p) = pL_1 + (pC_2 + y_2(p))^{-1}.$$

Looking into the transformer from the 50-ohm load gives the impedance

$$z_X(p) = n^2 \tilde{z}_X(p) = \frac{R_0}{R} \tilde{z}_X(p).$$

Normalizing to R_0 , the reflectance is

$$s_X(p) = \frac{z_X(p) - R_0}{z_X(p) + R_0} = \frac{\tilde{z}_X(p)/R - 1}{\tilde{z}_X(p)/R + 1}. \quad (13)$$

There are two transmission zeros at $p = \infty$. The expansion of the integrand at infinity exhibits this fact:

$$\begin{aligned} \log(s_X(p)^{-1}) &= \frac{A_1^\infty}{p} + \frac{A_3^\infty}{p^3} + \frac{A_4^\infty}{p^4} + \frac{A_5^\infty}{p^5} + \dots \\ &= \frac{2R}{L_1 p} + \frac{1}{p^3} \left\{ \frac{2R^3}{3L_1^3} - \frac{2R}{L_1^2 C_2} \right\} + \frac{1}{p^4} \frac{2R y_2(p)}{L_1^2 C_2^2} + \mathcal{O}[p^{-5}], \end{aligned}$$

provided the admittance $y_2(p)$ is bounded as $p \rightarrow \infty$. The leading coefficients now contain the load's resistor. Equation 10 computes the optimal K value assuming normalization by R_0 instead of 1 ohm. Consequently, Equations 11 and 12 compute the upper bound on the transducer power gain and lower bound on the VSWR—all normalized to R_0 . Figures 14 and 15 show the corresponding Fano bounds for this low-pass RLC circuit.

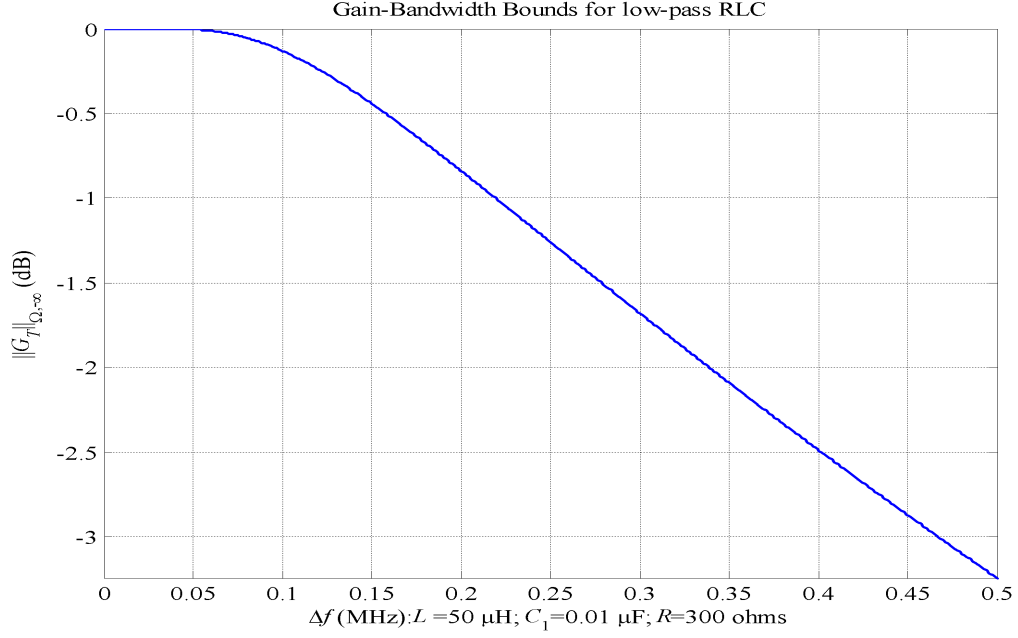


Figure 14: Upper bounds on gain as a function of bandwidth $\omega_c = 2\pi\Delta f$.

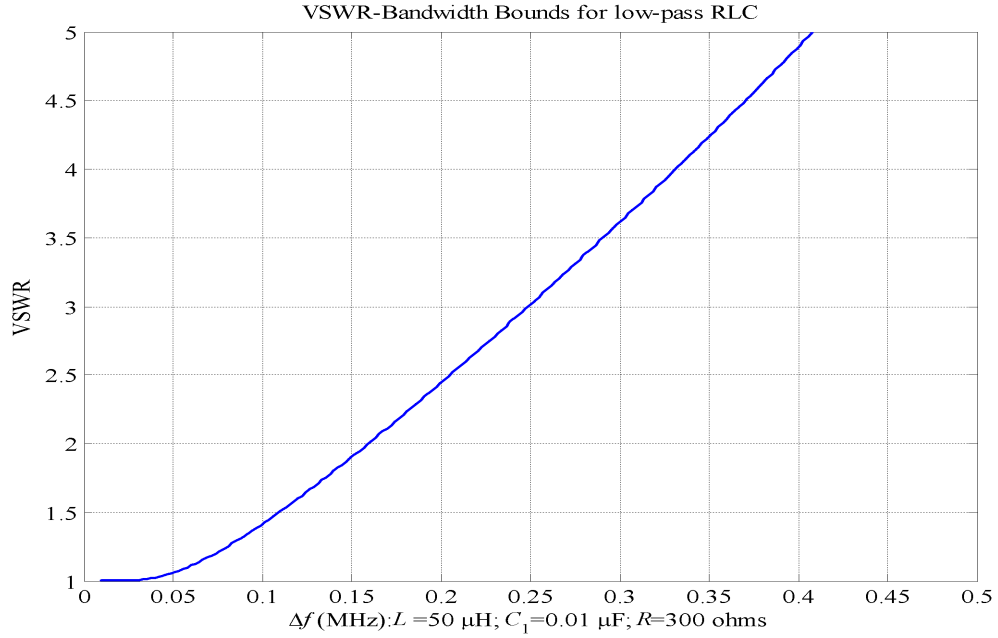


Figure 15: Lower bounds on VSWR as a function of bandwidth $\omega_c = 2\pi\Delta f$.

7 Microstrip Patch Antenna

A Fano analysis of a microstrip patch antenna [10] is based on the equivalent circuit of Figure 16. For reference, Figures 17 and 18 plot the impedance and reflectance of this circuit near resonance.

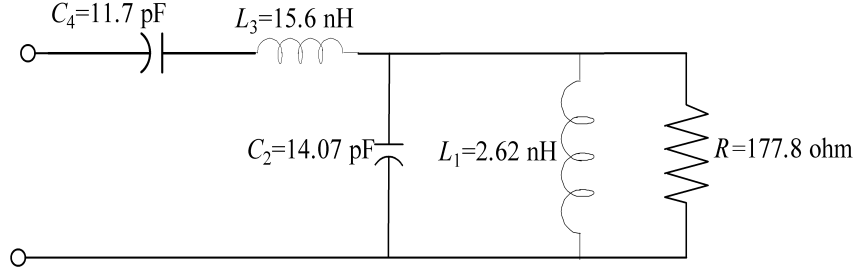


Figure 16: Microstrip patch antenna—equivalent circuit.

The Fano analysis starts by computing the transmission zeros. Let $S_X(p)$ denote the scattering matrix of the Darlington representation of the load. Port 1 looks in from the resistor. Port 2 is the input to the load. The transmission zeros are zeros of the (1,2) element of scattering matrix $S_X(p)$:

$$S_{X,12}(p) = \frac{2L_1C_4p^2}{C_2L_1L_3C_4p^4 + (2L_1C_4 + C_2L_1 + L_3C_4)p^2 + (C_2L_1C_4 + L_3L_1C_4)p^3 + (C_4 + LL_1)p + 1}.$$

This rational function has two transmission zeros at $p = \infty$ and two transmission zeros at $p = 0$. Rather than undertake this tedious algebra, a more transparent approach extracts the transmission zeros directly from the circuit diagram.

Theorem 4 [25, pages 165–167] *If either a ladder's shunt impedance is zero or its series admittance is zero, then the ladder has a transmission zero.*

Figure 16 shows that the shunt impedance shorts at $p = 0$ and at $p = \infty$. Likewise, the series admittance is an open circuit at both $p = 0$ and $p = \infty$. Theorem 4 identifies these four cases as transmission zeros. Because the degree of the circuit is 4, these are the only transmission zeros. The reflectance looking in from the resistor is

$$s_X(p) = \frac{z_X(p) - R_0}{z_X(p) + R_0} = \frac{\tilde{z}_X(p)/R - 1}{\tilde{z}_X(p)/R + 1},$$

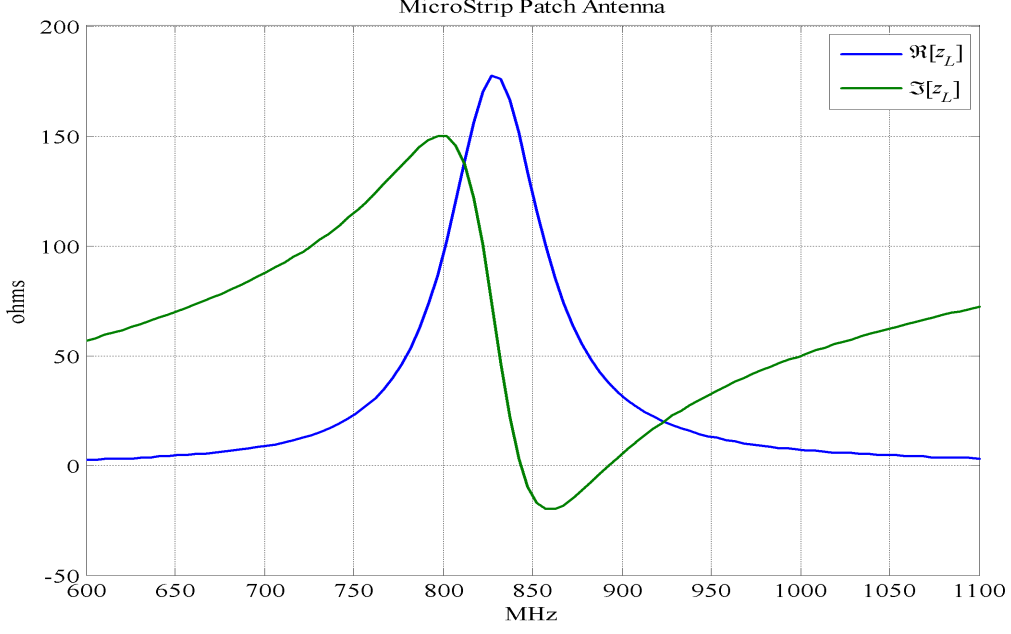


Figure 17: Microstrip patch antenna—impedance.

using the notation of Equation 13 to handle the resistor R . Expanding at $p = 0$:

$$\begin{aligned}
 \log(s_X(p)^{-1}) &= A_0^0 + A_1^0 p + A_3^0 p^3 + A_4^0 p^4 \dots \\
 &= -j\pi + 2\frac{L_1}{R}p - \frac{2L_1^2(3R^2C_2 + 3R^2C_4 - L_1)}{3R^3}p^3 \\
 &\quad + \frac{2z_2(p)c_4^2L_1^2}{R}p^4 + \mathcal{O}[p^{-5}],
 \end{aligned}$$

provided $z_2(p)$ is bounded as $p \rightarrow 0$. The two transmission zeros at $p = 0$ push the load $z_2(p)$ to the higher order terms. These two transmission zeros force the Fano integral constraints [9, Table II]

$$\int_0^\infty \omega^{-2} \log(|s_X(j\omega)|^{-1}) d\omega = \frac{\pi}{2} A_1^0 - \pi \sum p_m^{-1}, \quad (14)$$

$$\int_0^\infty \omega^{-4} \log(|s_X(j\omega)|^{-1}) d\omega = -\frac{\pi}{2} A_3^0 + \frac{\pi}{3} \sum p_m^{-3}, \quad (15)$$

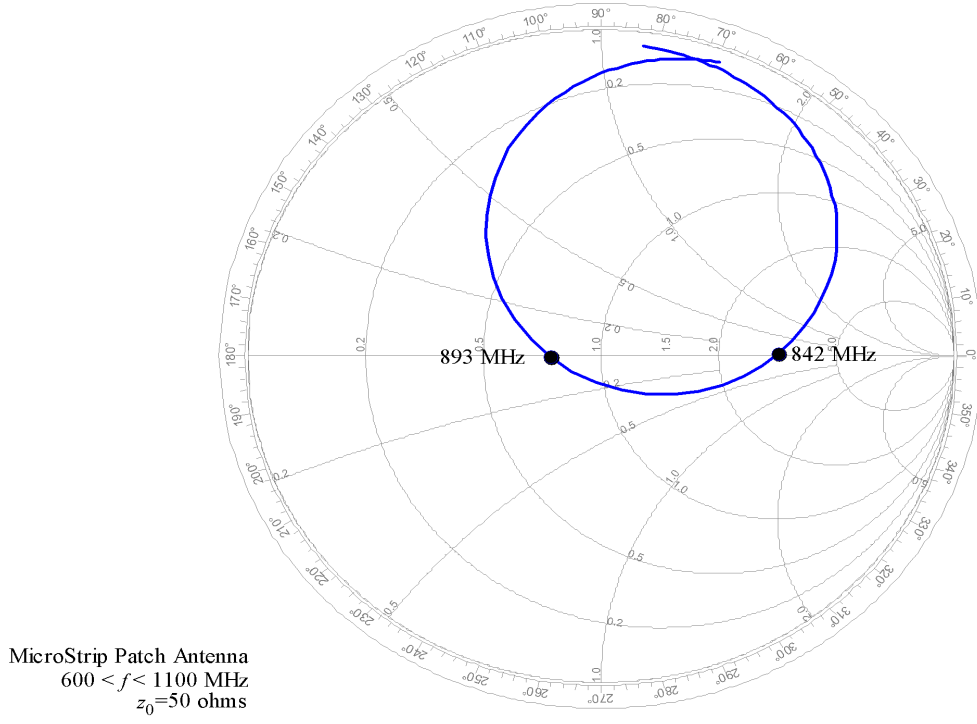


Figure 18: Microstrip patch antenna—reflectance.

where the p_m 's are the zeros of $s_X(p)$ that lie in the open right half plane. Expanding at $p = \infty$:

$$\begin{aligned}
 \log(s_X(p)^{-1}) &= A_0^\infty + \frac{A_1^\infty}{p} + \frac{A_3^\infty}{p^3} + \frac{A_4^\infty}{p^4} + \frac{A_5^\infty}{p^5} + \dots \\
 &= -j\pi + \frac{2}{C_2 R} \times \frac{1}{p} - \frac{2}{3} \frac{3L_1 R^2 C_2 + 3R^2 C_2 L_3 - L_1 L_3}{C_2^3 L_1 L_3 R^3} \times \frac{1}{p^3} \\
 &\quad + \frac{2z_2(p)}{C_2^2 R L_3^2} \times \frac{1}{p^4} + \mathcal{O}[p^{-5}],
 \end{aligned}$$

provided $z_2(p)$ is bounded as $p \rightarrow \infty$. The two transmission zeros at $p = \infty$ push the load $z_2(p)$ to the higher order terms. These two transmission zeros

force the Fano integral constraints [9, Table II]

$$\int_0^\infty \log(|s_X(j\omega)|^{-1})d\omega = \frac{\pi}{2}A_1^\infty - \pi \sum p_m, \quad (16)$$

$$\int_0^\infty \omega^2 \log(|s_X(j\omega)|^{-1})d\omega = -\frac{\pi}{2}A_3^\infty + \frac{\pi}{3} \sum p_m^3. \quad (17)$$

Again, the p_m 's are the zeros of $s_X(p)$ that lie in the open right half plane.

Denote the frequency band as $\Omega := [\omega_{\min}, \omega_{\max}]$. Bound the performance of the reflectance $s_X(p)$ on Ω as

$$\min\{\log(|s_X(j\omega)|^{-1}) : \omega \in \Omega\} =: \pi K/2.$$

Consequently, the reflectance $s_X(p)$ is bounded as

$$\log(|s_X(j\omega)|^{-1}) \geq \begin{cases} \pi K/2 & \omega_{\min} < |\omega| < \omega_{\max} \\ 0 & \text{otherwise} \end{cases}.$$

Inserting this lower bound into the Fano integrals produces the following inequalities:

$$\begin{aligned} \frac{\pi K}{2}(\omega_{\max} - \omega_{\min}) &\leq \int_0^\infty \log(|s_X(j\omega)|^{-1})d\omega, \\ \frac{\pi K}{6}(\omega_{\max}^3 - \omega_{\min}^3) &\leq \int_0^\infty \omega^2 \log(|s_X(j\omega)|^{-1})d\omega, \\ \frac{\pi K}{2}(\omega_{\min}^{-1} - \omega_{\max}^{-1}) &\leq \int_0^\infty \omega^{-2} \log(|s_X(j\omega)|^{-1})d\omega, \\ \frac{\pi K}{6}(\omega_{\min}^{-3} - \omega_{\max}^{-3}) &\leq \int_0^\infty \omega^{-4} \log(|s_X(j\omega)|^{-1})d\omega. \end{aligned}$$

Denote the zeros of $s_X(p)$ as $p_m = u_m + jv_m$. Because the sums are real, the Fano integral constraints force the equalities

$$\begin{aligned} \Re \left[\sum p_m \right] &= \sum u_m, \\ \Re \left[\sum p_m^3 \right] &= \sum u_m^3 - 3u_m v_m^2, \\ \Re \left[\sum p_m^{-1} \right] &= \sum \frac{u_m}{u_m^2 + v_m^2}, \\ \Re \left[\sum p_m^{-3} \right] &= \sum \frac{u_m(u_m^2 - 3v_m^2)}{(u_m^2 + v_m^2)^3}. \end{aligned}$$

Combining these inequalities with the Fano constraints (Equations 14, 15, 16, 17) produces the following inequalities:

$$\begin{aligned}
K(\omega_{\max} - \omega_{\min}) &\leq A_1^\infty - 2 \sum u_m, \\
K(\omega_{\max}^3 - \omega_{\min}^3) &\leq -3A_3^\infty + 2 \sum u_m(u_m^2 - 3v_m^2), \\
K(\omega_{\min}^{-1} - \omega_{\max}^{-1}) &\leq A_1^0 - 2 \sum \frac{u_m}{u_m^2 + v_m^2}, \\
K(\omega_{\min}^{-3} - \omega_{\max}^{-3}) &\leq -3A_3^0 + 2 \sum \frac{u_m(u_m^2 - 3v_m^2)}{(u_m^2 + v_m^2)^3}.
\end{aligned}$$

The goal is to maximize K subject to the inequalities determined by the zeros in the right half plane. Define the functions

$$\begin{aligned}
h_0(\mathbf{u}, \mathbf{v}) &:= (\omega_{\max} - \omega_{\min})^{-1} \left\{ A_1^\infty - 2 \sum u_m \right\}, \\
h_1(\mathbf{u}, \mathbf{v}) &:= (\omega_{\max}^3 - \omega_{\min}^3)^{-1} \left\{ -3A_3^\infty + 2 \sum u_m(u_m^2 - 3v_m^2) \right\}, \\
h_2(\mathbf{u}, \mathbf{v}) &:= (\omega_{\min}^{-1} - \omega_{\max}^{-1})^{-1} \left\{ A_1^0 - 2 \sum \frac{u_m}{u_m^2 + v_m^2} \right\}, \\
h_3(\mathbf{u}, \mathbf{v}) &:= (\omega_{\min}^{-3} - \omega_{\max}^{-3})^{-1} \left\{ -3A_3^0 + 2 \sum \frac{u_m(u_m^2 - 3v_m^2)}{(u_m^2 + v_m^2)^3} \right\}.
\end{aligned}$$

Maximizing K is equivalent to maximizing

$$\min\{h_0(\mathbf{u}, \mathbf{v}), h_1(\mathbf{u}, \mathbf{v}), h_2(\mathbf{u}, \mathbf{v}), h_3(\mathbf{u}, \mathbf{v})\}$$

subject to the constraints that $\mathbf{u} > 0$. Because $s_X(p)$ is a real rational function, its zeros p_m in the right half plane come in conjugate pairs. Coupled with the observation that the $h_k(\mathbf{u}, \mathbf{v})$'s are even functions in \mathbf{v} :

$$h_k(\mathbf{u}, -\mathbf{v}) = h_k(\mathbf{u}, \mathbf{v}),$$

the optimization domain can be restricted to $\mathbf{u} > 0$ and $\mathbf{v} \geq 0$. The following Lagrange multiplier is a classical approach:

$$\max\{h_0(\mathbf{u})\}$$

subject to the constraints that $\mathbf{u} > 0$, $\mathbf{v} \geq 0$ and

$$\begin{aligned}
g_1(\mathbf{u}) &:= h_1(\mathbf{u}) - h_0(\mathbf{u}) = 0, \\
g_2(\mathbf{u}) &:= h_2(\mathbf{u}) - h_0(\mathbf{u}) = 0, \\
g_3(\mathbf{u}) &:= h_3(\mathbf{u}) - h_0(\mathbf{u}) = 0.
\end{aligned}$$

The Lagrange multipliers take the form [17]

$$\nabla h_0 = \lambda_1 \nabla g_1 + \lambda_2 \nabla g_2 + \lambda_3 \nabla g_3,$$

or equivalently,

$$(1 + \lambda_1 + \lambda_2 + \lambda_3) \nabla h_0 = \lambda_1 \nabla h_1 + \lambda_2 \nabla h_2 + \lambda_3 \nabla h_3.$$

Although a symbolic manipulator can solve this algebraic system, and the p_m 's do decouple, the multipliers $\lambda_1, \lambda_2, \lambda_3$ and the number of p_m 's are confounding factors. Fortunately, the long and difficult algebraic analysis is evaded by exploiting the insights gained by the more robust approach of simply maximizing the function

$$K = \min\{h_0(\mathbf{u}, \mathbf{v}), h_1(\mathbf{u}, \mathbf{v}), h_2(\mathbf{u}, \mathbf{v}), h_3(\mathbf{u}, \mathbf{v})\}$$

subject to $\mathbf{u} \geq 0, \mathbf{v} \geq 0$, and a fixed number of p_m 's. For the rest of the discussion, it will be more convenient to use the same inequalities for the \mathbf{u} 's and the \mathbf{v} 's. Accordingly, this approach is developed and the insights gained can then be applied to the Lagrange multipliers.

Figure 19 shows a lower bound on VSWR as a function of fractional bandwidth while fixing the number of p_m 's to 1. Specifically, the function

$$K = \min\{h_0(u_1, v_1), h_1(u_1, v_1), h_2(u_1, v_1), h_3(u_1, v_1)\}$$

is maximized “over one zero” $p_1 = u_1 + jv_1$. Hence, the “Fano 1-bound” in the title of the plot. The VSWR is computed from the optimal K using Equation 12. The fractional bandwidth Δf determines the frequency band $[f_{\min}, f_{\max}]$ around the resonance $f_r = 843$ MHz as

$$\begin{aligned} f_{\min} &= f_r(1 - \Delta f/2), \\ f_{\max} &= f_r(1 + \Delta f/2). \end{aligned}$$

For comparison with the preceding plots, the fractional bandwidth $\Delta f = 0.5932$ approximates the interval $[600, 1100]$ MHz.

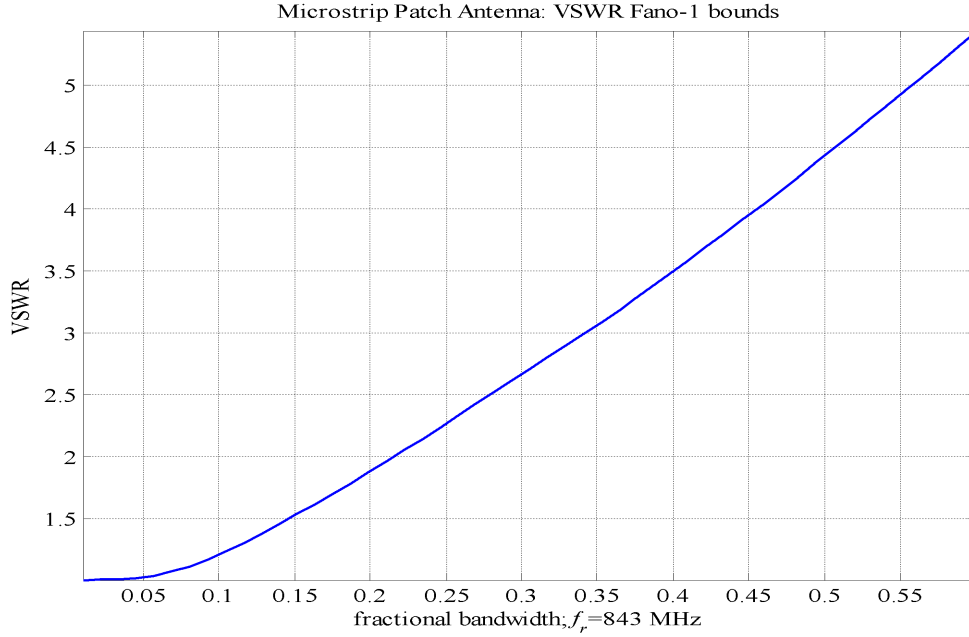


Figure 19: Microstrip patch antenna—Fano 1-bound.

Optimization of K over multiple zeros $(u_1, v_1, u_2, v_2, u_3, v_3, \dots)$ did not change the plot and leads to the natural conjecture that Figure 19 is the Fano bound. To address this conjecture, $K(u_1, v_1)$ is plotted in Figure 20. The plot is clipped to only show positive K values. The plot shows $K(u_1, v_1)$ is maximized on the v_1 axis.

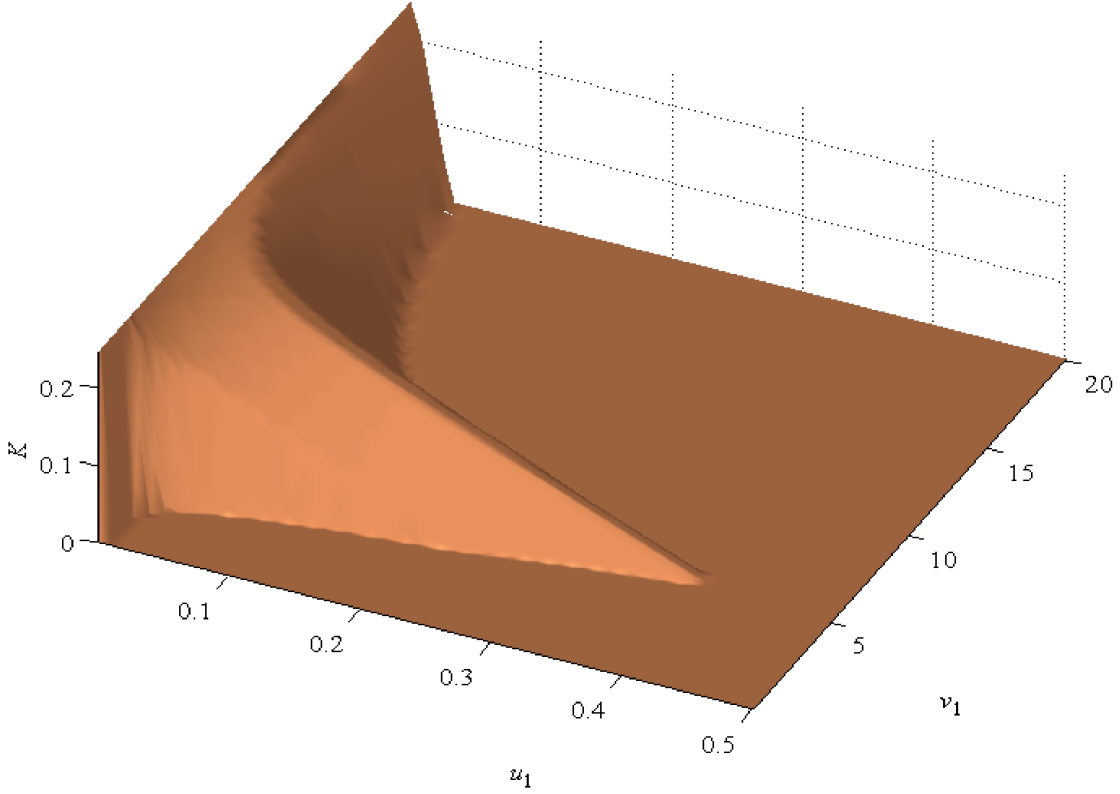


Figure 20: Microstrip patch antenna— K plot; 600–1100 MHz.

Examination of the functions $h_0(\mathbf{u}, \mathbf{v})$, $h_1(\mathbf{u}, \mathbf{v})$, $h_2(\mathbf{u}, \mathbf{v})$, and $h_3(\mathbf{u}, \mathbf{v})$ near the \mathbf{v} axis is listed in Table 5. The first numerical column evaluates the functions on the \mathbf{v} axis and shows all functions are constant for $\mathbf{u} = 0$. The last column lists gradient of each function on the \mathbf{v} axis with $\mathbf{v} > 0$. For clarity, the frequency scaling is omitted and these normalized functions are

denoted by the capital “ H ”:

$$\begin{aligned}
H_0(\mathbf{u}, \mathbf{v}) &:= A_1^\infty - 2 \sum u_m, \\
H_1(\mathbf{u}, \mathbf{v}) &:= -3A_3^\infty + 2 \sum u_m(u_m^2 - 3v_m^2), \\
H_2(\mathbf{u}, \mathbf{v}) &:= A_1^0 - 2 \sum \frac{u_m}{u_m^2 + v_m^2}, \\
H_3(\mathbf{u}, \mathbf{v}) &:= -3A_3^0 + 2 \sum \frac{u_m(u_m^2 - 3v_m^2)}{(u_m^2 + v_m^2)^3}.
\end{aligned}$$

This column shows that every component of the gradient in the neighborhood of the \mathbf{v} axis is decreasing in the \mathbf{u} directions. Because the functions are constant on the \mathbf{v} axis, this decrease forces the \mathbf{v} axis to be a local maximum of the K function. Because each component of the gradients are the same, the same shape of $K(u_1, v_1)$ of Figure 20 is replicated when plotting $K(\mathbf{u}, bfv)$. Consequently, the Fano 1-bounds of Figure 19 are the Fano bounds.

Table 5: Fano functions near the \mathbf{v} axis.

	$h_n(\mathbf{0}, \mathbf{v})$	$\partial H_n(\mathbf{0}, \mathbf{v})/\partial u_m$
h_0	0.2545	-2
h_1	0.2743	$-6v_m^2$
h_2	0.2444	$-2v_m^{-2}$
h_3	0.3814	$-6v_m^{-4}$

8 Ideal Dipole

If VSWR is plotted as a function of frequency, local minima identify local resonances. At each resonance, the local sublevel sets are intervals:

$$[f_1, f_2] = \{f \in \mathbb{R} : \text{VSWR}(f) \leq S\}.$$

Consequently, one definition of bandwidth Δf is based on these sublevel sets of the VSWR [21, Eq. 5]:

$$\Delta f := \frac{f_2 - f_1}{f_r},$$

where f_r is a resonant frequency in the frequency band $[f_1, f_2]$.

Hujanen, Holmberg, and Sten obtain an upper bound on the bandwidth Δf for a small antenna with radius a and wavenumber k [15, Eq. 4]:

$$\Delta f \leq \frac{(ka)^3}{1 + (ka)^2} \frac{S^2 - 1}{2S}, \quad (18)$$

provided the input impedance is modeled by a single pole. Figure 21 shows two schematics of the impedance models for an ideal dipole.

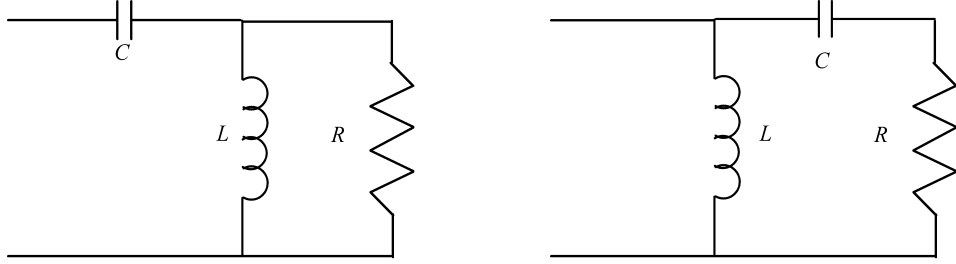


Figure 21: Impedance models of the TM₁ and TE₁ modes of the ideal dipole; $C = a\epsilon_0 = a \times 8.85$ (pF), $L = a\mu_0 = a \times 1.26$ (μ H), $R = \sqrt{\mu_0/\epsilon_0} = 377.3233$ (ohms).

Resonance for TM_1 occurs when $|z_L(j\omega)|$ is minimum [7, page 81]:

$$\begin{aligned}\omega_r &= \frac{R(L + RC^{1/2}(R^2C + 2L)^{1/2})^{1/2}}{L^{1/2}(R^4C^2 + 2LR^2 - L^2)^{1/2}} \\ &= \frac{1}{a} \frac{(1 + 3^{1/2})^{1/2}}{2^{1/2}\sqrt{\mu_0\epsilon_0}} \\ &= \frac{c}{a}(1 + 3^{1/2})^{1/2}2^{-1/2}.\end{aligned}$$

In terms of frequency,

$$f_r = \frac{55.70}{a}.$$

Figure 22 plots the impedance of the TM_1 mode. Figure 23 plots the associated VSWR. Both plots show that bandwidth is a local definition. The pole at $f = 0$ and the flat rolloff at the high frequencies distort the symmetry of f_1 and f_2 with respect to f_r . Figure 24 plots the dipole's reflectance on the Smith chart.

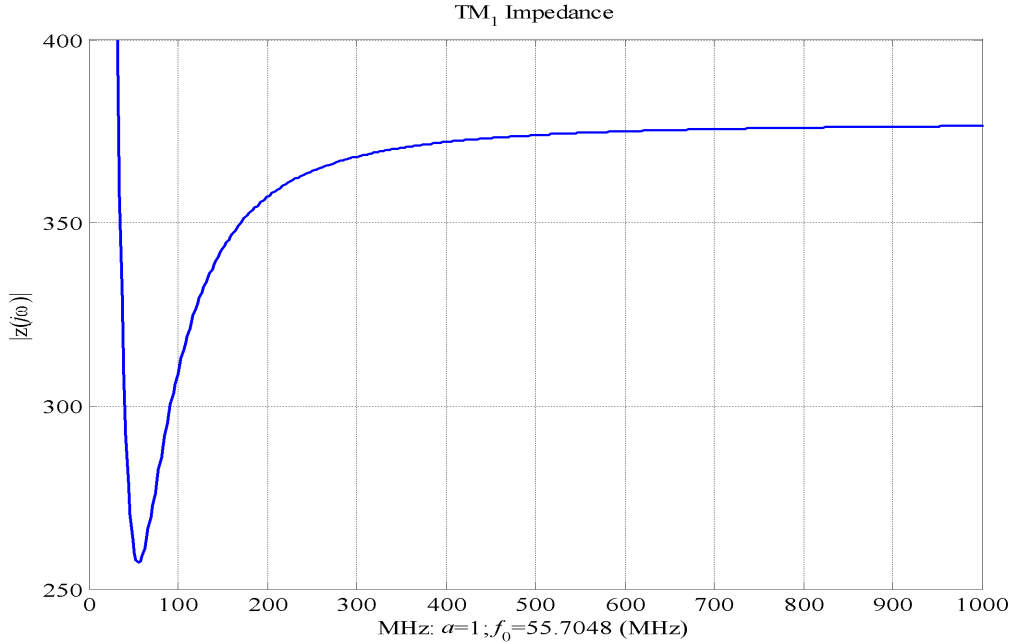


Figure 22: Ideal dipole—impedance of the TM_1 mode.

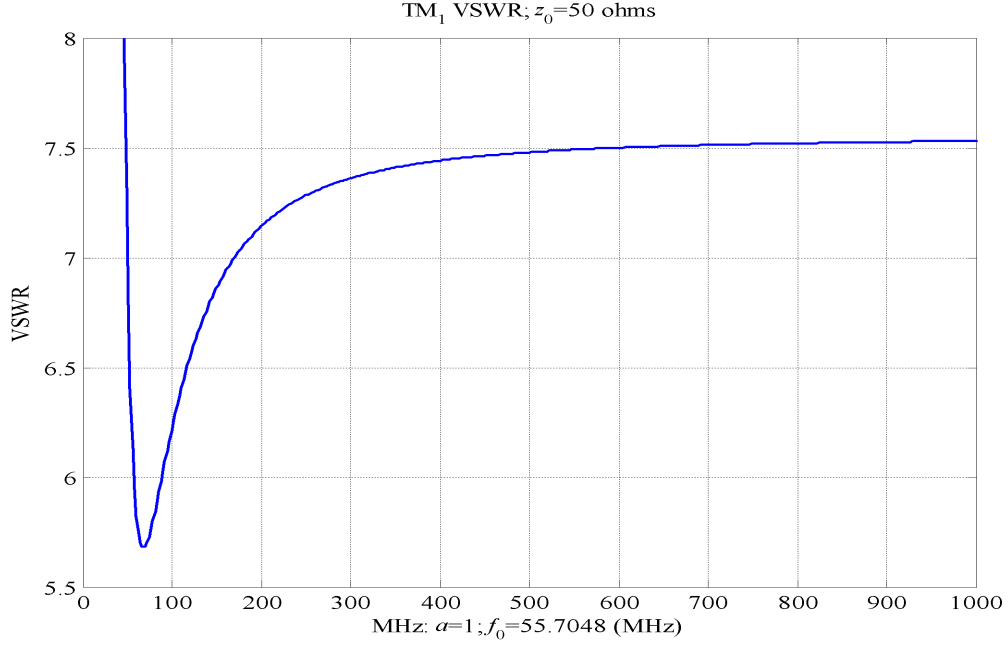


Figure 23: Ideal dipole—VSWR of the TM_1 mode.

Figure 21 shows that the shunt inductor is a short circuit at $p = 0$ and that the series capacitor is an open circuit at $p = 0$. Theorem 4 identifies these two cases as transmission zeros. Because the degree of the circuit is 2, these are the only transmission zeros. The reflectance looking in from the resistor and normalized to R_0 is

$$s_X(p) = \frac{z_X(p) - R_0}{z_X(p) + R_0} = \frac{\tilde{z}_X(p)/R - 1}{\tilde{z}_X(p)/R + 1},$$

using the notation of Equation 13 to handle the resistor R . In this case, the impedance looking in from the resistor is

$$\tilde{z}_X(p) = ((pL)^{-1} + ((pC)^{-1} + z_2(p))^{-1})^{-1},$$

where $z_2(p)$ is the impedance looking out from the antenna into the matching

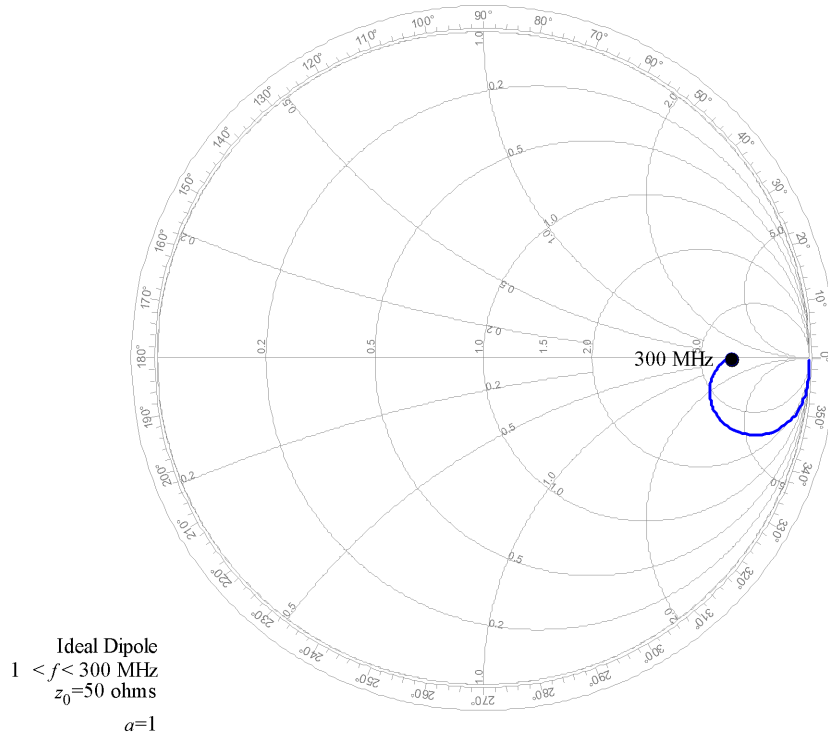


Figure 24: Ideal dipole—reflectance.

circuit. Expanding at $p = 0$:

$$\begin{aligned}
 \log(s_X(p)^{-1}) &= A_0^0 + A_1^0 p + A_3^0 p^3 + A_4^0 p^4 \dots \\
 &= -j\pi + 2\frac{L}{R}p - \frac{2L^2(3R^2C - L)}{3R^3}p^3 \\
 &\quad + \frac{2z_2(p)C^2L^2}{R}p^4 + \mathcal{O}[p^{-5}],
 \end{aligned}$$

provided $z_2(p)$ is bounded as $p \rightarrow 0$. As expected, the transmission zeros at $p = 0$ pushes the load $z_2(p)$ into the higher order terms.

These transmission zeros force the Fano integral constraints [9, Table II]

$$\int_0^\infty \omega^{-2} \log(|s_X(j\omega)|^{-1}) d\omega = \frac{\pi}{2} A_1^0 - \pi \sum p_m^{-1}, \quad (19)$$

$$\int_0^\infty \omega^{-4} \log(|s_X(j\omega)|^{-1}) d\omega = -\frac{\pi}{2} A_3^0 + \frac{\pi}{3} \sum p_m^{-3}, \quad (20)$$

where the p_m 's are the zeros of $s_X(p)$ that lie in the open right half plane. Denote the frequency band as $\Omega := [\omega_{\min}, \omega_{\max}]$. Bound the performance of the reflectance $s_X(p)$ on Ω as

$$\min\{\log(|s_X(j\omega)|^{-1}) : \omega \in \Omega\} =: \pi K/2.$$

Consequently, the reflectance $s_X(p)$ is bounded on the entire frequency axis as

$$\log(|s_X(j\omega)|^{-1}) \geq \begin{cases} \pi K/2 & \omega_{\min} < |\omega| < \omega_{\max} \\ 0 & \text{otherwise} \end{cases}.$$

Inserting this lower bound into the Fano integrals produces the inequalities:

$$\begin{aligned} \frac{\pi K}{2}(\omega_{\min}^{-1} - \omega_{\max}^{-1}) &\leq \int_0^\infty \omega^{-2} \log(|s_X(j\omega)|^{-1}) d\omega = \frac{\pi}{2} A_1^0 - \pi \sum p_m^{-1}, \\ \frac{\pi K}{6}(\omega_{\min}^{-3} - \omega_{\max}^{-3}) &\leq \int_0^\infty \omega^{-4} \log(|s_X(j\omega)|^{-1}) d\omega = -\frac{\pi}{2} A_3^0 + \frac{\pi}{3} \sum p_m^{-3}. \end{aligned}$$

Denote the zeros of $s_X(p)$ as $p_m = u_m + jv_m$. Because the sums are real, the Fano integral constraints force the equalities:

$$\begin{aligned} \Re \left[\sum p_m^{-1} \right] &= \sum \frac{u_m}{u_m^2 + v_m^2}, \\ \Re \left[\sum p_m^{-3} \right] &= \sum \frac{u_m(u_m^2 - 3v_m^2)}{(u_m^2 + v_m^2)^3}. \end{aligned}$$

Combining these inequalities with the Fano integrals produces

$$\begin{aligned} K(\omega_{\min}^{-1} - \omega_{\max}^{-1}) &\leq A_1^0 - 2 \sum \frac{u_m}{u_m^2 + v_m^2}, \\ K(\omega_{\min}^{-3} - \omega_{\max}^{-3}) &\leq -3A_3^0 + 2 \sum \frac{u_m^3 - 3u_m v_m^2}{(u_m^2 + v_m^2)^3}. \end{aligned}$$

The goal is to maximize K subject to the inequalities determined by the zeros in the right half plane. Define

$$\begin{aligned} h_0(\mathbf{u}, \mathbf{v}) &:= (\omega_{\min}^{-1} - \omega_{\max}^{-1})^{-1} \left\{ A_1^0 - 2 \sum \frac{u_m}{u_m^2 + v_m^2} \right\}, \\ h_1(\mathbf{u}, \mathbf{v}) &:= (\omega_{\min}^{-3} - \omega_{\max}^{-3})^{-1} \left\{ -3A_3^0 + 2 \sum \frac{u_m^3 - 3u_m v_m^2}{(u_m^2 + v_m^2)^3} \right\}. \end{aligned}$$

The Fano bounds are computed by maximizing

$$K = h_0(\mathbf{u}, \mathbf{v})$$

subject to the constraints that $\mathbf{u} \geq 0$, $\mathbf{v} \geq 0$ and that

$$0 = h_1(\mathbf{u}, \mathbf{v}) - h_0(\mathbf{u}, \mathbf{v}),$$

where the “ \geq ” is used to simplify the discussion. In terms of Lagrange multipliers, the Lagrangian can be written as

$$L(\mathbf{u}, \mathbf{v}) := h_0(\mathbf{u}, \mathbf{v}) - \lambda \{h_1(\mathbf{u}, \mathbf{v}) - h_0(\mathbf{u}, \mathbf{v})\}.$$

The Lagrange multiplier theorem identifies local extremum as stationary points of the Lagrangian or, equivalently [17, page 243]

$$(1 + \lambda)\nabla h_0 = \lambda\nabla h_1,$$

provided the points are regular. Because each vector component of the Lagrangian is the same equation, the same roots apply to all components and the resulting four roots are tabulated in Table 6.

Table 6: Extrema of the Lagrangian without positivity constraints.

u_m	v_m
$\sqrt{3}\sqrt{-\lambda(1+\lambda)}W$	0
$-\sqrt{3}\sqrt{-\lambda(1+\lambda)}W$	0
0	$\sqrt{\lambda(1+\lambda)}W$
0	$-\sqrt{\lambda(1+\lambda)}W$

$$W := -\frac{\sqrt{w_{\min}^2 + w_{\max}^2} + w_{\min} w_{\max} w_{\min}}{w_{\min}^2 \lambda + w_{\max}^2 \lambda + w_{\max}^2 + w_{\max} w_{\min} \lambda + w_{\min} w_{\max} + w_{\min}^2}.$$

What is fascinating about these solutions is that the roots are parameterized by the frequency band and the multiplier—it appears that the load does not affect these roots. However, the load does enter in the roots through the multiplier λ selected to enforce the constraint equation. The positivity of u and v forces two cases listed in Table 7.

Table 7: Positive extrema of the Lagrangian.

u	v	λ
$\sqrt{3}\sqrt{-\lambda(1+\lambda)} W $	0	$-1 < \lambda < 0$
0	$\sqrt{\lambda(1+\lambda)} W $	$\lambda < -1$ or $\lambda > 0$

However, this complicated dance through the inequalities can be avoided and more insight gained by considering the plot of $K(u_1, v_1)$. Figure 25 corroborates Table 7 by showing the maximum of $K(u_1, v_1)$ lie on both axis with the maximum on the v_1 axis.

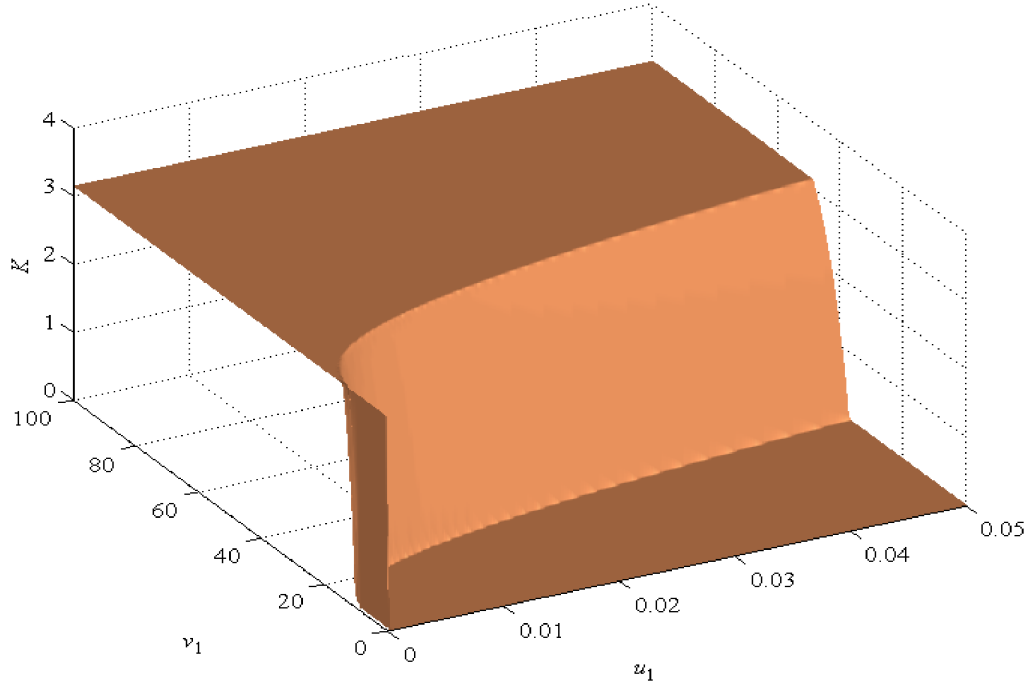


Figure 25: Ideal dipole— $K(u_1, v_1)$ plot.

Because the components of the gradients ∇h_0 and ∇h_1 yield the same form, Table 7 forces the maximum on the \mathbf{v} axis using these Fano functions:

$$h_0(0, \mathbf{v}) = \frac{A_1^0}{\omega_{\min}^{-1} - \omega_{\max}^{-1}} = \frac{2}{\omega_{\min}^{-1} - \omega_{\max}^{-1}} \times \frac{L}{R},$$

$$h_1(0, \mathbf{v}) = -\frac{3A_3^0}{\omega_{\min}^{-3} - \omega_{\max}^{-3}} = \frac{6}{\omega_{\min}^{-3} - \omega_{\max}^{-3}} \times \frac{L^2(3R^2C - L)}{3R^3}.$$

Figure 26 compares this Fano bound for the VSWR against the Fano 1-bound computed by numerically optimizing $K(u_1, v_1)$. Consequently, the analysis and numerical simulations argue that this plot does show the Fano bounds.

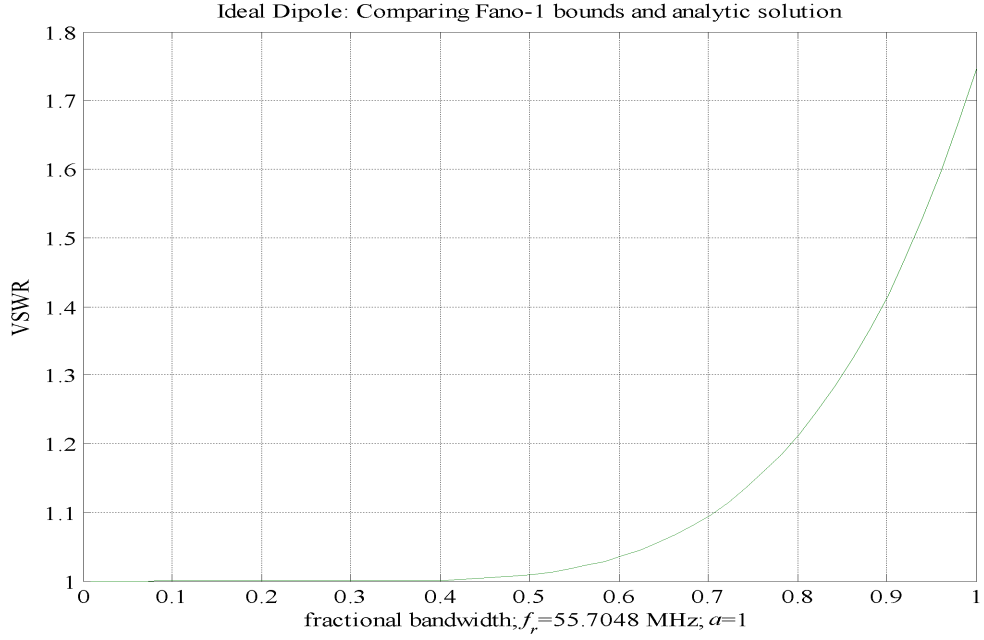


Figure 26: Ideal dipole—Fano bounds.

9 Automating the Fano Bounds

The preceding analysis demonstrates several issues must be addressed to automate the Fano bounds.

Rational Load: Basic to the Fano analysis is that the load is a rational function—not sampled impedances. Mapping sampled data to a bounded real rational function is a substantial problem in approximation theory.

Darlington’s Representation: The second step of the Fano analysis requires that the Darlington representation be determined from the load to compute the scattering matrix $S_X(p)$ and the Fano reflectance $s_X(p)$.

Transmission Zeros: The third step of the Fano analysis requires the transmission zeros of $S_X(p)$. Computing zeros of rational functions is always tricky. An intermediate approach applicable to antenna design would restrict the analysis to transmission zeros at $p = 0$ and $p = \infty$.

Fano Functions: The fourth step is to generate the Fano functions $h_0(\mathbf{u}, \mathbf{v})$, $h_1(\mathbf{u}, \mathbf{v})$, \dots associated with each transmission zero. A symbolic manipulator can compute a running expansion of $\log(s_X(p)^{-1})$ and halt when $z_2(p)$ appears in the expansion. A program could generate a “Fano file” that encodes each of these functions and compute

$$K = \min\{h_0(\mathbf{u}, \mathbf{v}), h_1(\mathbf{u}, \mathbf{v}), \dots\}.$$

Maximizing K : The fifth step of the Fano analysis is to maximize K . The preceding step has written the Fano functions in an M-file. Figure 20 shows the usual problems with finding a good starting point and crawling to a maximum on non-differentiable surface.

In summary, automating the Fano bounds appears possible, provided

- A Darlington representation of the load is computable.
- High-quality transmission zeros are computable.

A Fano-Bode Integrals

The Fano-Bode integrals are computed in [9, Table I]. This appendix re-derives Fano's result when the transmission zeros are at $p = \infty$. The derivation reveals Fano's adroit choice of the analytic windows that peel off the reflectance coefficients.

Assume the Fano reflectance $s_X(p)$ is a real, rational function with expansion at $p = \infty$ [9, Eq. 9]

$$\log(s_X(p)^{-1}) = j\beta + \frac{A_1^\infty}{p} + \frac{A_3^\infty}{p^3} + \dots + \frac{A_{2N+1}^\infty}{p^{2N+1}} + \frac{A_{2N+2}^\infty}{p^{2N+2}} \dots,$$

where the A_n^∞ 's are real and β is either 0 or $-\pi$ depending on the sign of $s_X(p)$ at infinity. Assume that $s_X(p)$ does not vanish on $j\mathbb{R}$. Let p_1, \dots, p_M denote the zeros of $s_X(p)$ in open right half plane \mathbb{C}_+ . The Fano-Bode integral is

$$\int_0^\infty \omega^{2n} \log(|s_X(j\omega)|^{-1}) d\omega = (-1)^n \frac{\pi}{2} \left\{ A_{2n+1}^\infty - \frac{2}{2n+1} \sum p_m^{2n+1} \right\},$$

for $n = 0, 1, \dots, N$.

Proof: Define the Blaschke function [22]:

$$B(p) := \prod_{m=1}^M \frac{p - p_m}{p + p_m}.$$

Because the zeros are in the open right half plane \mathbb{C}_+ , $B(p)$ is analytic on $\overline{\mathbb{C}}_+$. Because the zeros are either real or come in conjugate pairs, $B(p)$ is real. Define $\epsilon = \text{sign}[\lim_{p \rightarrow \infty} s(p)]$ and set

$$S_X(p) := \epsilon B(p)^{-1} s_X(p).$$

Observe $S_X(p)$ is real, analytic on $\overline{\mathbb{C}}_+$, and has no finite zeros in $\overline{\mathbb{C}}_+$. Consider integrating over the contour C_r in over the contour of Figure 27.

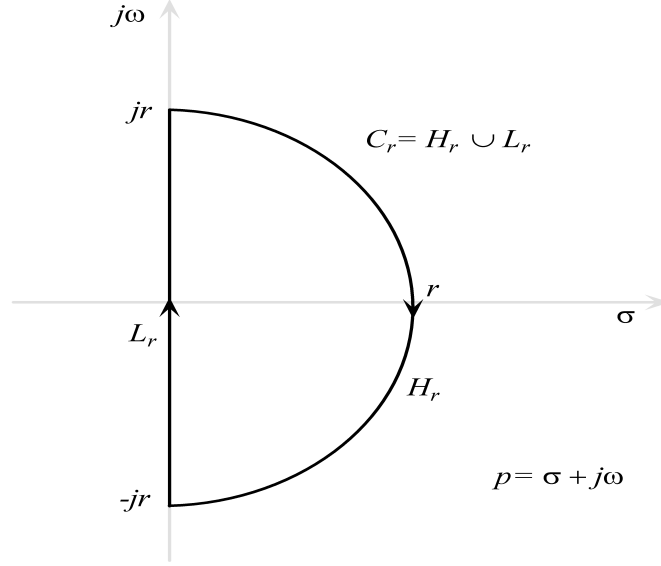


Figure 27: Contour C_r , line segment L_r , half circle H_r .

Cauchy's Theorem [22, Theorem 10.35] computes

$$\begin{aligned}
 0 &= \int_{C_r} p^{2n} \log(S_X(p)^{-1}) dp \\
 &= \int_{C_r} p^{2n} \log(\epsilon s_X(p)^{-1}) dp + \int_{C_r} p^{2n} \log(B(p)) dp. \quad (21)
 \end{aligned}$$

The first integral on the right side of Equation 21 decomposes over the contour as

$$\begin{aligned}
 \int_{C_r} p^{2n} \log(\epsilon s_X(p)^{-1}) dp &= \int_{-r}^r (j\omega)^{2n} \log(\epsilon s_X(j\omega)^{-1}) j d\omega \\
 &\quad + \int_{H_r} p^{2n} \log(\epsilon s_X(p)^{-1}) dp.
 \end{aligned}$$

Because $s_X(p)$ is real,

$$\log(\epsilon s_X(j\omega)) = \log(|s_X(j\omega)|) + j \arg[\epsilon s_X(j\omega)]$$

with $\log(|s_X(j\omega)|)$ an even function and $\arg[\epsilon s_X(j\omega)]$ an odd function. Consequently, the odd part integrates out over the integral on L_r :

$$\int_{-r}^r (j\omega)^{2n} \log(s_X(j\omega)^{-1}) j d\omega = j(-1)^n \int_{-r}^r \omega^{2n} \log(|s_X(j\omega)|^{-1}) d\omega.$$

Because

$$\log(|s_X(j\omega)|^{-1}) = (-1)^N \frac{A_{2N+2}^\infty}{\omega^{2N+2}} + \dots$$

as $|\omega| \rightarrow \infty$, the integral converges to the well-defined integral:

$$\lim_{r \rightarrow \infty} \int_{-r}^r (j\omega)^{2n} \log(s_X(j\omega)^{-1}) d\omega = (-1)^n \int_{-\infty}^{\infty} \omega^{2n} \log(|s_X(j\omega)|^{-1}) d\omega$$

for $n = 0, \dots, N$. The integral on the half circle H_r is evaluated using the asymptotic expansion:

$$\begin{aligned} & \int_{H_r} p^{2n} \log(\epsilon s_X(p)^{-1}) dp \\ &= \int_{H_r} p^{2n} \left\{ \frac{A_1^\infty}{p} + \frac{A_3^\infty}{p^3} + \dots + \frac{A_{2N+1}^\infty}{p^{2N+1}} + \frac{A_{2N+2}^\infty}{p^{2N+2}} \dots \right\} dp. \end{aligned}$$

Consider the case when $n = 0$:

$$\begin{aligned} & \int_{H_r} \log(\epsilon s_X(p)^{-1}) dp \\ &= \int_{H_r} \left\{ \frac{A_1^\infty}{p} + \frac{A_3^\infty}{p^3} + \dots + \frac{A_{2N+1}^\infty}{p^{2N+1}} + \frac{A_{2N+2}^\infty}{p^{2N+2}} \dots \right\} dp \\ &= A_1^\infty \log(p) - \frac{A_3^\infty}{2p^2} - \dots - \frac{A_{2N+1}^\infty}{2Np^{2N}} + \mathcal{O}[p^{-(2N+1)}] \Big|_{p=+jr}^{-jr} \\ &= -j\pi A_1^\infty. \end{aligned}$$

When $n = N$:

$$\begin{aligned} & \int_{H_r} p^{2N} \log(\epsilon s_X(p)^{-1}) dp \\ &= \int_{H_r} p^{2N} \left\{ \frac{A_1^\infty}{p} + \frac{A_3^\infty}{p^3} + \dots + \frac{A_{2N+1}^\infty}{p^{2N+1}} + \frac{A_{2N+2}^\infty}{p^{2N+2}} \dots \right\} dp \\ &= \int_{H_r} \left\{ A_1^\infty p^{2N-1} + A_3^\infty p^{2N-3} + \dots + \frac{A_{2N+1}^\infty}{p} + \mathcal{O}[p^{-2}] \right\} dp \\ &= A_1^\infty \frac{p^{2N}}{2N} + A_3^\infty \frac{p^{2N-2}}{2N-2} + \dots + A_{2N+1}^\infty \log(p) + \mathcal{O}[p^{-1}] \Big|_{p=+jr}^{-jr} \\ &= -j\pi A_{2N+1}^\infty. \end{aligned}$$

Gathering the results, the first integral on the right of Equation 21 decomposes over the contour as

$$\begin{aligned} & \int_{C_r} p^{2n} \log(\epsilon s_X(p)^{-1}) dp \\ &= (-1)^n \int_{-\infty}^{\infty} \omega^{2n} \log(|s_X(j\omega)|^{-1}) d\omega - j\pi A_{2n+1}^{\infty}. \end{aligned} \quad (22)$$

The second integral on the right side of Equation 21 decomposes over the contour as

$$\int_{C_r} p^{2n} \log(B(p)) dp = \int_{-r}^r (j\omega)^{2n} \log(B(j\omega)) j d\omega + \int_{H_r} p^{2n} \log(B(p)) dp.$$

Because $\log(B(j\omega)) = j\arg[B(j\omega)]$ and $\arg[g(j\omega)]$ an odd function, the line integral is zero. The integral on the half circle is evaluated from the expansion

$$\begin{aligned} B(p) &= \sum_{m=1}^M \log\left(\frac{p - p_m}{p + p_m}\right) \\ &= \sum_{m=1}^M \log\left(\frac{1 - p_m/p}{1 + p_m/p}\right) \\ &= -2 \sum_{m=1}^M \frac{p_m}{p} + \frac{1}{3} \left(\frac{p_m}{p}\right)^3 + \frac{1}{5} \left(\frac{p_m}{p}\right)^5 + \frac{1}{7} \left(\frac{p_m}{p}\right)^7 + \dots \end{aligned}$$

as $p \rightarrow \infty$. Consider the case when $n = 0$:

$$\begin{aligned} & \int_{H_r} \log(B(p)) dp \\ &= -2 \sum_{m=1}^M \int_{H_r} \left\{ \frac{p_m}{p} + \frac{1}{3} \left(\frac{p_m}{p}\right)^3 + \frac{1}{5} \left(\frac{p_m}{p}\right)^5 + \frac{1}{7} \left(\frac{p_m}{p}\right)^7 + \dots \right\} dp \\ &= \sum_{m=1}^M \left[-2p_m \log(p) + \frac{1}{3} \frac{p_m^3}{p^2} + \frac{1}{10} \frac{p_m^5}{p^4} + \frac{1}{21} \frac{p_m^7}{p^6} + \dots \right] \Bigg|_{p=+jr}^{-jr} \\ &= j2\pi \sum_{m=1}^M p_m. \end{aligned}$$

When $n = 1$,

$$\int_{H_r} p^2 \log(B(p)) dp = j \frac{2}{3} \pi \sum_{m=1}^M p_m^3.$$

When $n = 2$,

$$\int_{H_r} p^4 \log(B(p)) dp = j \frac{2}{5} \pi \sum_{m=1}^M p_m^5.$$

Gathering these results,

$$\int_{C_r} p^{2n} \log(B(p)) dp = j \frac{2}{2n+1} \pi \sum_{m=1}^M p_m^{2n+1}. \quad (23)$$

Substitute Equations 23 and 22 into Equation 21:

$$0 = j(-1)^n \int_{-\infty}^{\infty} \omega^{2n} \log(|s_X(j\omega)|^{-1}) d\omega - j\pi A_{2n+1}^{\infty} + j \frac{2}{2n+1} \pi \sum_{m=1}^M p_m^{2n+1}.$$

///

B Scattering Measurements to a Darlington Representation

Section 9 pointed out that the Fano Method requires a Darlington representation of the load. A real-world load is typically measured over a frequency band. Extracting a credible Darlington representation from these sampled reflectances is challenging. The state-space representation of a passive, lumped N -port provides a physically credible model automatically disgorges a Darlington representation. Figure 28 motivates the discussion by approximating a measured antenna reflectance (blue line) using a state space model (green line). Although the finer features are lost, this state-space model of the data used only two inductors, two capacitors, and a single resistor to obtain a worst-case fit over 2–30 MHz.

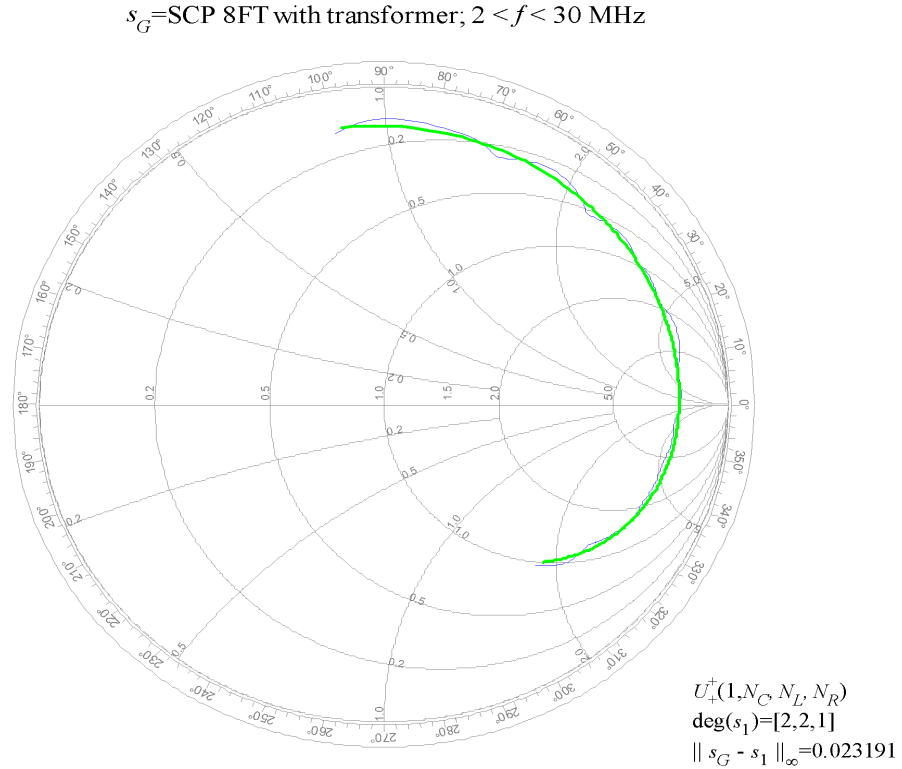


Figure 28: Surface Current Probe approximation with degree 4.

Figure 29 illustrates the state-space representation of a passive, lumped N -port. The figure shows that by pulling the d reactive elements and the r lossy elements into the *augmented load* $S_L(p)$, what is left is an $(N+d+r)$ -port consisting of the wires, transformers, and gyrators. This *constant* $(N+d+r)$ -port has *constant* scattering matrix S_a , called the *augmented scattering matrix*. The N -port is obtained by looking into Ports 1, 2, \dots , N of the augmented scattering matrix S_a while its remaining ports are terminated in the augmented load $S_L(p)$. That is, $S(p)$ is the image of the augmented load viewed through the augmented scattering matrix.

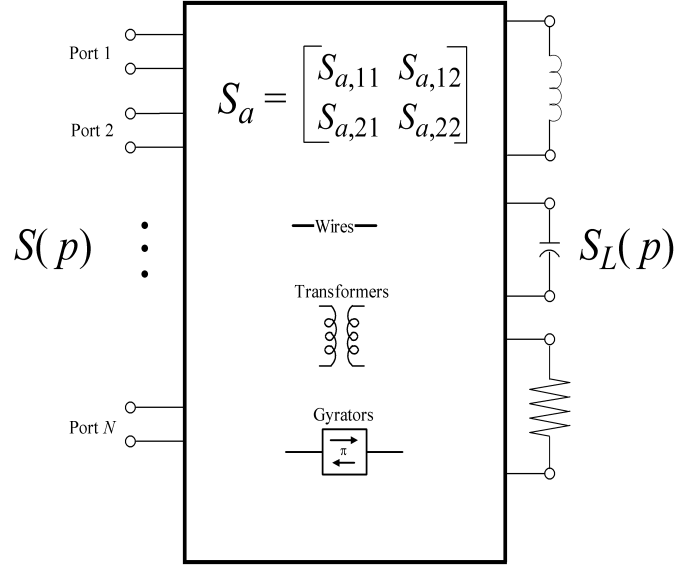


Figure 29: State-space representation of a passive, lumped N -port containing d reactive elements and r resistors.

After introducing the necessary definitions, Theorem 5 gives the precise statement of the *state-space representation*.

Definition 1 Let $S \in \Re \overline{B}H^\infty(\mathbb{C}_+, \mathbb{C}^{N \times N})$ and be rational [26, page 91]:

- The normal rank of $S(p)$ is

$$r[S(p)] := \text{rank}[I_N - S(-p)^T S(p)].$$

- The skew-symmetric rank of $S(p)$ is

$$g[S(p)] := \frac{1}{2} \text{rank}[S(p) - S(p)^T].$$

- Let the K distinct poles of $S(p)$ be denoted as p_k . Let $\deg(S(p); p_k)$ denote the largest order to which $p = p_k$ appears in any minor of $S(p)$. The Smith-McMillan degree of $S(p)$ is

$$\deg_{\text{SM}}[S(p)] := \sum_{k=1}^K \deg(S(p); p_k).$$

Theorem 5 (State-Space [26, pages 90–93]) *Every lumped, passive, causal, time-invariant N -port admits a scattering matrix $S(p)$ and conversely. If $S(p)$ has Smith-McMillan degree d and normal rank r , then $S(p)$ admits the following state-space representation:*

$$S(p) = \mathcal{F}(S_a, S_L; p) := S_{a,11} + S_{a,12}S_L(p)(I_{d+r} - S_{a,22}S_L)^{-1}S_{a,21},$$

where the augmented load is

$$S_L(p) = \begin{bmatrix} q \times I_{N_L} & 0 & 0 \\ 0 & -q \times I_{N_C} & 0 \\ 0 & 0 & 0 \times I_r \end{bmatrix}, \quad \left(q = \frac{p-1}{p+1} \right),$$

and $N_L + N_C = d$. The augmented scattering matrix is

$$S_a = \begin{bmatrix} S_{a,11} & S_{a,12} \\ S_{a,21} & S_{a,22} \end{bmatrix} \begin{matrix} N \\ d+r \\ N & d+r \end{matrix}$$

is a constant, real, orthogonal matrix. If the N -port is lossless, then $r = 0$. If the N -port is reciprocal, then S_a is symmetric: $S_a^T = S_a$.

Although a scattering matrix $S(p)$ has lots of representations, the following list shows that the state-space representation extracts a lot of the N -port's structure [26, page 91], [19]. For brevity, “in any passive N -port” means the N -port of Theorem 5.

Resistors. The number of resistors N_R in any passive N -port exceeds the normal rank:

$$N_R \geq r[S(p)].$$

Moreover, of all the N -ports that have $S(p)$ as their scattering matrix, there exists at least one having exactly $r[S(p)]$ resistors.

Reactive. The number of inductors N_L and capacitors N_C in any passive N -port exceeds the Smith-McMillan degree:

$$N_L + N_C \geq \deg_{\text{SM}}[S(p)].$$

Moreover, of all the N -ports that have $S(p)$ as their scattering matrix, there exists at least one N -port having exactly this many inductors and capacitors.

Gyrators. The number of gyrators in any passive N -port exceeds the skew-symmetric rank:

$$N_G \geq g[S(p)].$$

Wohlers [26, page 92] remarks that only in the case that $g[S(p)] = 0$ or that $S(p)$ is symmetric, can an N -port can be found that is reciprocal or contains no gyrators.

Theorem 5 provides a numerically efficient parameterization of the scattering matrices corresponding to the lumped, passive N -ports independent of any circuit topology. Denote the class of lumped, *lossless* N -ports of degree d as

$$U^+(N, d) := \{S \in U^+(N) : \deg_{\text{SM}}[S(p)] \leq d\}.$$

Next, introduce the group of $M \times M$ orthogonal matrices:

$$\mathcal{O}[M] := \{S \in \mathbb{R}^{M \times M} : S^T S = I_M\}.$$

Theorem 5 determines that $U^+(N, d)$ is the orbit of a *fixed* reactive load under the action of the orthogonal $\mathcal{O}[N + d]$.

Theorem 6 *Any augmented load,*

$$S_L(p) = \frac{p-1}{p+1} \begin{bmatrix} I_{N_L} & 0 \\ 0 & -I_{N_C} \end{bmatrix} \quad (N_L + N_C = d)$$

has orbit

$$U^+(N, d) = \mathcal{F}(\mathcal{O}[N + d], S_L).$$

Sweeping over the orthogonal group $\mathcal{O}[N + d]$ generates all lumped, lossless, N -ports of degree d .

It is known that $U^+(N, d)$ is compact, so best approximations from $U^+(N, d)$ do exist. Unfortunately, little is known regarding the characterization of best approximations from $U^+(N, d)$ and the rate of convergence as $d \rightarrow \infty$. Therefore, the remainder of this section simply shows the quality of numerical approximations for several real-world antennas. The goal is to obtain a Darlington's representation for a given reflectance s_G . The first step is to compute the best approximation from the orbit of a 1-ohm resistor under the action of the lossless 2-ports:

$$\min\{\|s_G - s_1\|_{\Omega, \infty} : s_1 \in U(N; N_L, N_C, N_R)\},$$

where the notation returns to the decomposition of Theorem 5. The number of ports is denoted by N . Because the reflectance s_G is a scalar, $N = 1$. The number of inductors and capacitors is denoted by N_L and N_C , respectively. The number of resistors is denoted by N_R . Because a Darlington's representation is being computed, $N_R = 1$. The Darlington's representation takes the reflectance s_1 at Port 1 with the understanding that the resistor is located at Port 2. The plots reports the reflectance as $s_1 \in U(1, N_L, N_C, N_R)$. The definition of "degree" is slightly expanded as $\deg[s_1] = [N_L \ N_C \ 1]$ to make explicit that a the single resistor is used. The caption to each plot still reports the degree d as the number of reactive elements.

Figures 30 and 31 show the quality of this approximation to the reflectance of the AOC21B measurements [23]. The reflectance is plotted in blue and shows two large resonances and dozens of small resonances. The approximations are the green lines and a visually appealing fit is obtained with a 16-degree 2-port.

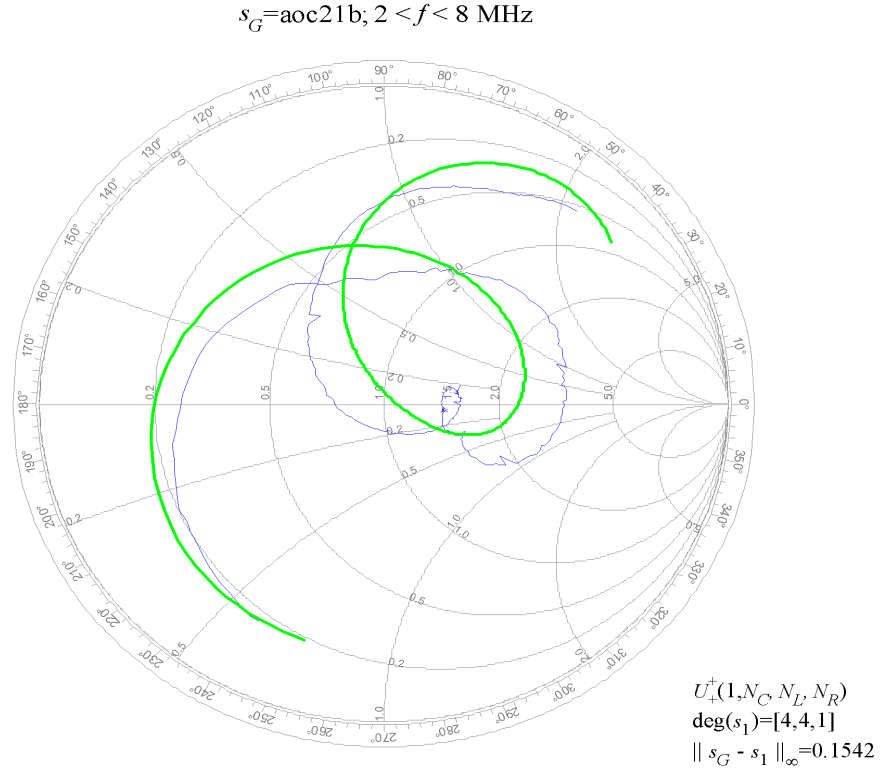


Figure 30: AOC21B and approximation with degree 8.

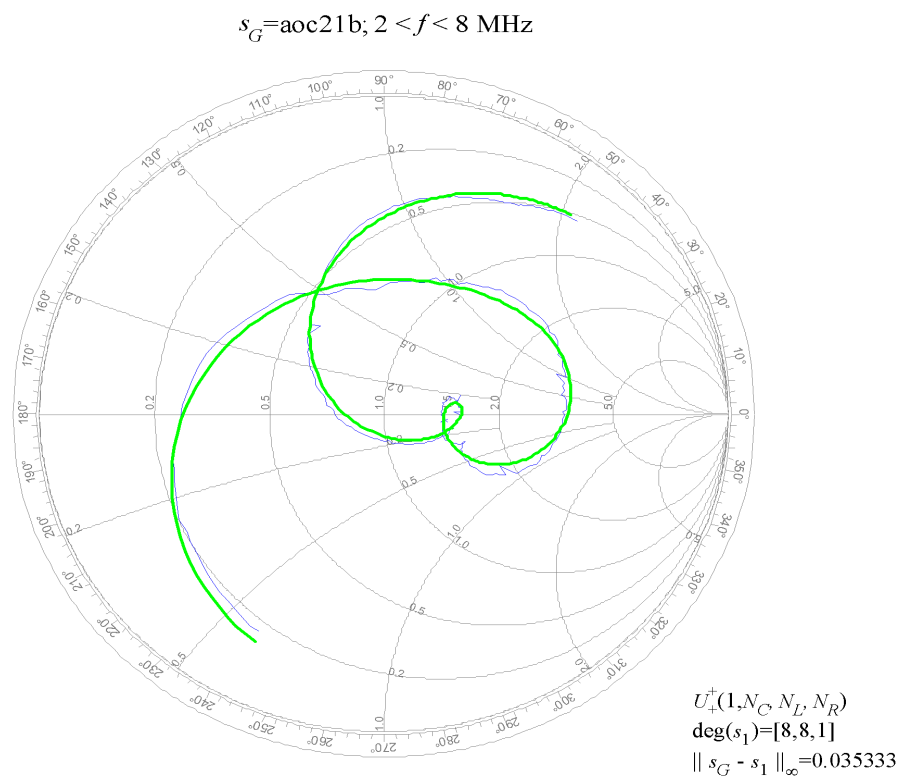


Figure 31: AOC21B and approximation with degree 16.

The CNV77Z measurements (blue line) are less complex than the preceding AOC21B measurements. Relatively good approximations are obtained for small degree d as shown in Figures 32 and 33. Nevertheless, Figure 34 shows that the small resonance is not approximated until degree 16 is reached.

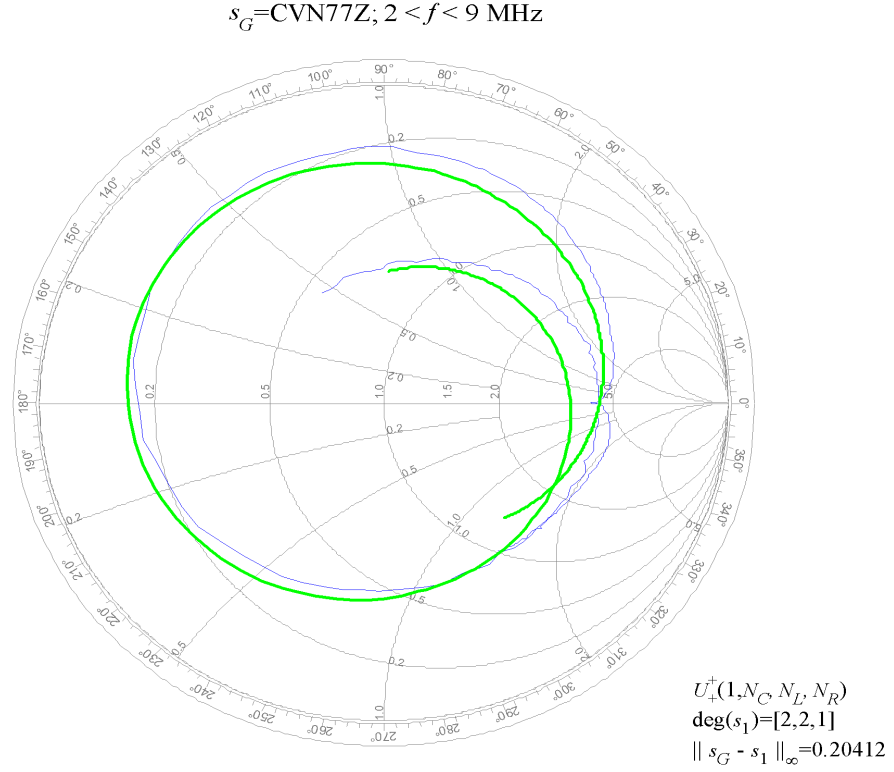


Figure 32: CVN77Z approximation with degree 4.

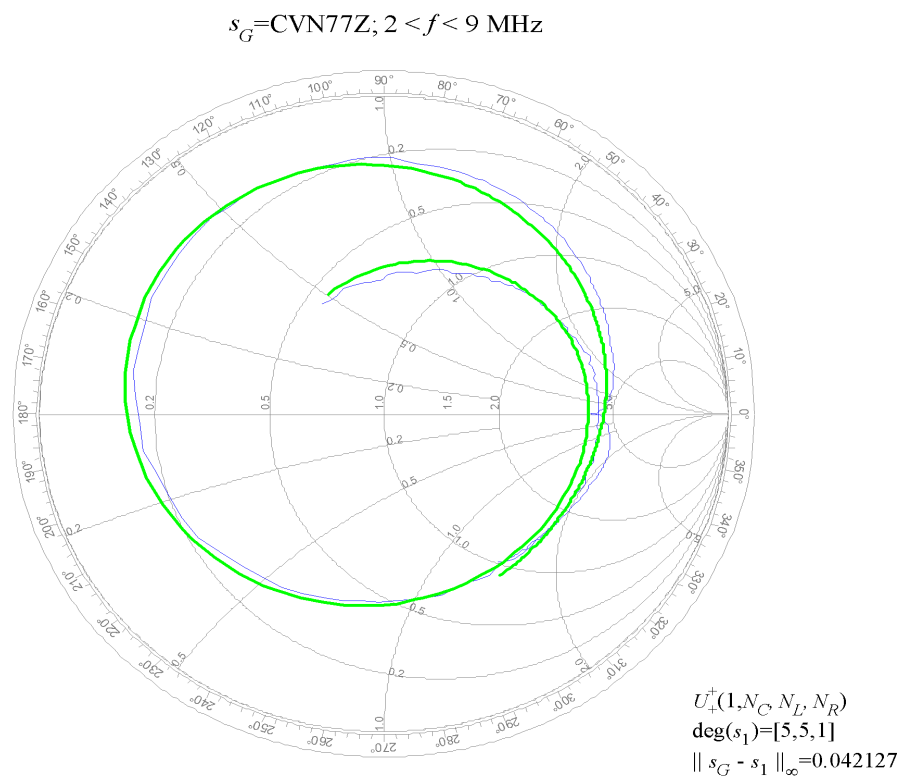


Figure 33: CVN77Z approximation with degree 10.

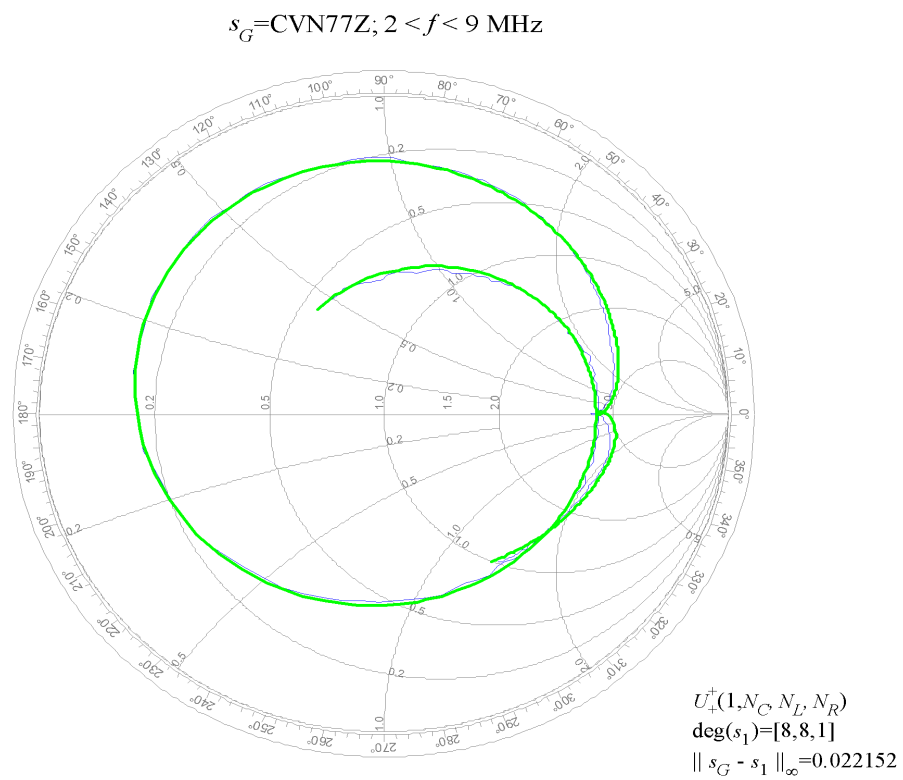


Figure 34: CVN77Z approximation with degree 16.

The Surface Current Probe started this discussion. Figure 28 shows the fit when the antenna has been “pre-processed” by a transformer. The transformer pulls the reflectance further into the Smith chart a fine structure appears. Comparison with Figure 35 is interesting because both plots have the same degree and the measurements differ only by a transformer. If the transformer was ideal, the errors $\|s_G - s_1\|_\infty$ should be identical because the lossless 2-ports sweep over all transformers—all ideal transformers. However, the real-world transformer induces resonances that prevent a tight fit.

s_G =SCP 8FT; no transformer; $2 < f < 9$ MHz

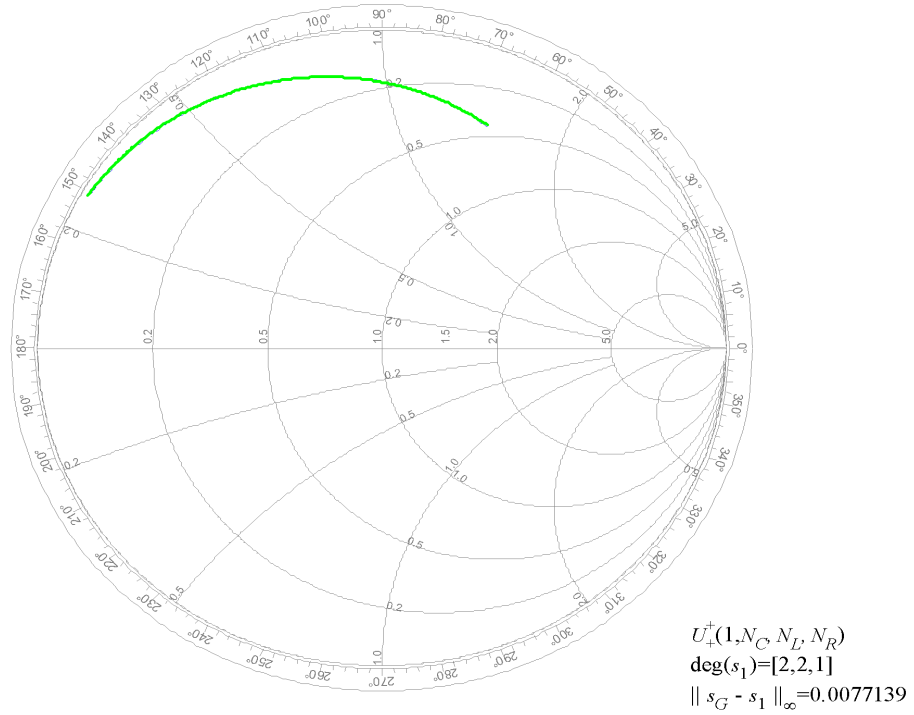


Figure 35: Surface Current Probe (no transformer) approximation with degree 4.

References

- [1] Allen, J. C. and Dennis Healy [2003] Nehari's Theorem and Electric Circuits, in *Modern Signal Processing*, Edited by Daniel Rockmore and Dennis Healy, Springer-Verlag.
- [2] Analui, Behnam and Ali Hajimiri [2004] Bandwidth Enhancement for Transimpedance Amplifiers *IEEE Journal of Solid-State Circuits*, 39(8), pages 1263–1270.
- [3] Baher, H. [1984] *Synthesis of Electrical Networks*, John Wiley & Sons.
- [4] Balabanian, Norman & Theodore A. Bickart [1981] *Linear Network Theory*, Matrix Publishers, Inc., Beaverton, OR.
- [5] Carlin, Herbert J. and Pier Paolo Civalleri [1997] *Wideband Circuit Design*, CRC Press, NY, NY.
- [6] Choi, B.G. Lee, Y.S. Park, C.S. Yoon, K.S. [2000] Super Low Noise C-band PHEMT MMIC Low Noise Amplifier with Minimum Input Matching Network, *Electronics Letters*, 36, pages 1627–1629.
- [7] Edminister, Joseph A. [1965] *Electric Circuits*, Schaum's Outline.
- [8] Dobrowolski, Janusz A. & Wojciech Ostrowski [1996] *Computer-Aided Analysis, Modeling, and Design of Microwave Networks*, Artech House, Boston, MA.
- [9] Fano, R.M. [1950] Theoretical Limitations on the Broadband Matching of Arbitrary Impedances, *Journal of the Franklin Institute*, 249(1) pages 57–83, and 249(2), pages 139–154.
- [10] Ghorbani, A., Raed A. Abd-Alhameed, Neil J. McEwan, D. Zho [2006] An Approach for Calculating the Limiting Bandwidth-Reflection Coefficient Product for Microstrip Patch Antennas, *IEEE Transactions on Antenna and Propagation*, 54(4), pages 1328–1331.
- [11] Gonzalez, Guillermo [1997] *Microwave Transistor Amplifiers*, Second Edition, Prentice Hall, Upper Saddle River, NJ.

- [12] Goodwin, Graham C. Stefan F. Graebe, Mario E. Salgado [2001] *Control System Design*, Prentice-Hall, Inc.
- [13] Gustafsson, Mats and Sven Nordebo [2005] *Bandwidth Q Factor, and Resonance Models of Antennas*, LUNDX/(TEAT-7138)/1-16(2005), Department of Electrosience, Lund Institute of Technology, Sweden.
- [14] Helton, J. W. [1982] Non-Euclidean Functional Analysis and Electronics, *Bulletin of the American Mathematical Society*, Volume 7, Number 1, pages 1–64.
- [15] Hujanen, Aro; Jan Holmberg; Johan Carl-Erik Sten [2005] Bandwidth Limitations of Impedance Matched Ideal Dipoles, *IEEE Transactions on Antenna and Propagation*, 53(10), pages 3236–3239.
- [16] Lau, Buon Kiong, Jørgen Bach Andersen, Gerhard Kristensson, Adreas F. Molisch [2006] Impact of Matching Network on Bandwidth of Compact Antenna Arrays, *IEEE Transactions on Antennas and Propagation*, 54(11), pages 3225–3237.
- [17] Luenberger, David G. [1969] *Optimization by Vector Space Methods*, John Wiley & Sons, Inc., New York, NY.
- [18] Morris, M.L. Jensen, M.A. [2005] Network Model for MIMO Systems with Coupled Antennas and Noisy Amplifiers, *IEEE Transactions on Antennas and Propagation*, 53(1), pages 545–552.
- [19] Newcomb, Robert W. [1966] *Linear Multiport Synthesis*, McGraw-Hill Electronic Sciences Series, New York, NY.
- [20] Pozar, David M. [1998] *Microwave Engineering*, third edition, Prentice-Hall.
- [21] Pues, Huge F. and Antoine R. Van De Capelle [1989] An Impedance-Matching Technique for Increasing the Bandwidth of Microstrip Antennas, *IEEE Transactions on Antenna and Propagation*, 37(11), pages 1345–1354.
- [22] Rudin, Walter [1974] *Real and Complex Analysis*, second edition, McGraw-Hill, Inc., New York, NY.

- [23] Schwartz, David F. and J.C. Allen [2000] Computing Performance Bounds for Wideband Impedance Matching, *17th Annual Review of Progress in Applied Computational Electromagnetics*, Monterey, CA pages 594–599.
- [24] Sokolov, A.G., Babak, L.I. Babak [1999] Examples of Numerical Solution of the Fano Gain-Bandwidth Limitation Problem for Different Load Types, *Application of the Conversion Research Results for International Cooperation*, SIBCONVERS'99, pages 236–238.
- [25] Temes, Gabor C., Jack W. LaParta [1977] *Introduction to Circuit Synthesis and Design*, McGraw-Hill Book Company, NY, NY.
- [26] Wohlers, M. R. [1965] Gain-bandwidth Limitations for Physically Realizable Systems, *IEEE Transactions on Circuits and Systems*, 12(3), pages 329–333.
- [27] Yorko, J. J. [1992] A Broadband Manpack Antenna for SINCGARS Range Extension, *Proceedings of the Tactical Communications Conference*, Volume 1, pages 297–301.
- [28] Youla, D.C. [1964] A New Theory of Broad-Band Matching, *IEEE Transactions on Circuit Theory*, CT-11(1), pages 30–50.
- [29] Young, Jeffrey L., Ryan S. Adams, Benton O'Neil [2005] Bandwidth Optimization of an Integrated Microstrip Circulator and Antenna Assembly: Part One, *preprint*.
- [30] Zhu, Lizhong and Yihong Qi [1996] A Novel Approach to Evaluating The Gain-Bandwidth Potential of Antennas, *Antennas and Propagation Society International Symposium*, Baltimore, MD, USA, Volume: 3, pages 2058–2061.

Approved for public release; distribution is unlimited.